Search for the neutral current top quark decay $t \to Zc$ using the ratio of Z-boson + 4 jets to W-boson + 4 jets production

T. Aaltonen,[24] J. Adelman,[14] T. Akimoto,[56] B. Álvarez González,[12,t] S. Amerio,[44b,44a] D. Amidei,[35] A. Anastassov,[39] A. Annovi,[20] J. Antos,[15] G. Apollinari,[18] A. Apresyan,[49] T. Arisawa,[58] A. Artikov,[16] W. Ashmanskas,[18] A. Attal,[4] A. Aurisano,[54] F. Azfar,[43] P. Azzurri,[47b,47a] W. Badgett,[18] A. Barbaro-Galtieri,[29] V. E. Barnes,[49] B. A. Barnett,[26] V. Bartsch,[31] G. Bauer,[33] P.-H. Beauchemin,[34] F. Bedeschi,[47a] D. Beecher,[31] S. Behari,[26] G. Bellettini,[47b,47a] J. Bellinger,[60] D. Benjamin,[17] A. Beretvas,[18] J. Beringer,[29] A. Bhatti,[51] M. Binkley,[18] D. Bisello,[44b,44a] I. Bizjak,[31,y] R. E. Blair,[2] C. Blocker,[7] B. Blumenfeld,[26] A. Bocci,[17] A. Bodek,[50] V. Boisvert,[50] G. Bolla,[49] D. Bortoletto,[49] J. Boudreau,[48] A. Boveia,[11] B. Brau,[11,b] A. Bridgeman,[25] L. Brigliadori,[44a] C. Bromberg,[36] E. Brubaker,[14] J. Budagov,[16] H. S. Budd,[50] S. Budd,[25] S. Burke,[18] K. Burkett,[18] G. Busetto,[44b,44a] P. Bussey,[22] A. Buzatu,[34] K. L. Byrum,[2] S. Cabrera,[17,v] C. Calancha,[32] M. Campanelli,[36] M. Campbell,[35] F. Canelli,[14,18] A. Canepa,[46] B. Carls,[25] D. Carlsmith,[60] R. Carosi,[47a] S. Carrillo,[19,o] S. Carron,[34] B. Casal,[12] M. Casarsa,[18] A. Castro,[6b,6a] P. Catastini,[47c,47a] D. Cauz,[55b,55a] V. Cavaliere,[47c,47a] M. Cavalli-Sforza,[4] A. Cerri,[29] L. Cerrito,[31,p] S. H. Chang,[28] Y. C. Chen,[1] M. Chertok,[8] G. Chiarelli,[47a] G. Chlachidze,[18] F. Chlebana,[18] K. Cho,[28] D. Chokheli,[16] J. P. Chou,[23] G. Choudalakis,[33] S. H. Chuang,[53] K. Chung,[13] W. H. Chung,[60] Y. S. Chung,[50] T. Chwalek,[27] C. I. Ciobanu,[45] M. A. Ciocci,[47c,47a] A. Clark,[21] D. Clark,[7] G. Compostella,[44a] M. E. Convery,[18] J. Conway,[8] M. Cordelli,[20] G. Cortiana,[44b,44a] C. A. Cox,[8] D. J. Cox,[8] F. Crescioli,[47b,47a] C. Cuenca Almenar,[8,v] J. Cuevas,[12,t] R. Culbertson,[18] J. C. Cully,[35] D. Dagenhart,[18] M. Datta,[18] T. Davies,[22] P. de Barbaro,[50] S. De Cecco,[52a] A. Deisher,[29] G. De Lorenzo,[4] M. Dell'Orso,[47b,47a] C. Deluca,[4] L. Demortier,[51] J. Deng,[17] M. Deninno,[6a] P. F. Derwent,[18] G. P. di Giovanni,[45] C. Dionisi,[52b,52a] B. Di Ruzza,[55b,55a] J. R. Dittmann,[5] M. D'Onofrio,[4] S. Donati,[47b,47a] P. Dong,[9] J. Donini,[44a] T. Dorigo,[44a] S. Dube,[53] J. Efron,[40] A. Elagin,[54] R. Erbacher,[8] D. Errede,[25] S. Errede,[25] R. Eusebi,[18] H. C. Fang,[29] S. Farrington,[43] W. T. Fedorko,[14] R. G. Feild,[61] M. Feindt,[27] J. P. Fernandez,[32] C. Ferrazza,[47d,47a] R. Field,[19] G. Flanagan,[49] R. Forrest,[8] M. J. Frank,[5] M. Franklin,[23] J. C. Freeman,[18] H. J. Frisch,[14] I. Furic,[19] M. Gallinaro,[52a] J. Galyardt,[13] F. Garberson,[11] J. E. Garcia,[21] A. F. Garfinkel,[49] K. Genser,[18] H. Gerberich,[25] D. Gerdes,[35] A. Gessler,[27] S. Giagu,[52b,52a] V. Giakoumopoulou,[3] P. Giannetti,[47a] K. Gibson,[48] J. L. Gimmell,[50] C. M. Ginsburg,[18] N. Giokaris,[3] M. Giordani,[55b,55a] P. Giromini,[20] M. Giunta,[47b,47a] G. Giurgiu,[26] V. Glagolev,[16] D. Glenzinski,[18] M. Gold,[38] N. Goldschmidt,[19] A. Golossanov,[18] G. Gomez,[12] G. Gomez-Ceballos,[33] M. Goncharov,[33] O. González,[32] I. Gorelov,[38] A. T. Goshaw,[17] K. Goulianos,[51] A. Gresele,[44b,44a] S. Grinstein,[23] C. Grosso-Pilcher,[14] R. C. Group,[18] U. Grundler,[25] J. Guimaraes da Costa,[23] Z. Gunay-Unalan,[36] C. Haber,[29] K. Hahn,[33] S. R. Hahn,[18] E. Halkiadakis,[53] B.-Y. Han,[50] J. Y. Han,[50] F. Happacher,[20] K. Hara,[56] D. Hare,[53] M. Hare,[57] S. Harper,[43] R. F. Harr,[59] R. M. Harris,[18] M. Hartz,[48] K. Hatakeyama,[51] C. Hays,[43] M. Heck,[27] A. Heijboer,[46] B. Heinemann,[29] J. Heinrich,[46] C. Henderson,[33] M. Herndon,[60] J. Heuser,[27] S. Hewamanage,[5] D. Hidas,[17] C. S. Hill,[11,d] D. Hirschbuehl,[27] A. Hocker,[18] S. Hou,[1] M. Houlden,[30] S.-C. Hsu,[29] B. T. Huffman,[43] R. E. Hughes,[40] U. Husemann,[61] M. Hussein,[36] J. Huston,[36] J. Incandela,[11] G. Introzzi,[47a] M. Iori,[52b,52a] A. Ivanov,[8] E. James,[18] D. Jang,[13] B. Jayatilaka,[17] E. J. Jeon,[28] M. K. Jha,[6a] S. Jindariani,[18] W. Johnson,[8] M. Jones,[49] K. K. Joo,[28] S. Y. Jun,[13] J. E. Jung,[28] T. R. Junk,[18] T. Kamon,[54] D. Kar,[19] P. E. Karchin,[59] Y. Kato,[42,m] R. Kephart,[18] J. Keung,[46] V. Khotilovich,[54] B. Kilminster,[18] D. H. Kim,[28] H. S. Kim,[28] H. W. Kim,[28] J. E. Kim,[28] M. J. Kim,[20] S. B. Kim,[28] S. H. Kim,[56] Y. K. Kim,[14] N. Kimura,[56] L. Kirsch,[7] S. Klimenko,[19] B. Knuteson,[33] B. R. Ko,[17] K. Kondo,[58] D. J. Kong,[28] J. Konigsberg,[19] A. Korytov,[19] A. V. Kotwal,[17] M. Kreps,[27] J. Kroll,[46] D. Krop,[14] N. Krumnack,[5] M. Kruse,[17] V. Krutelyov,[11] T. Kubo,[56] T. Kuhr,[27] N. P. Kulkarni,[59] M. Kurata,[56] S. Kwang,[14] A. T. Laasanen,[49] S. Lami,[47a] S. Lammel,[18] M. Lancaster,[31] R. L. Lander,[8] K. Lannon,[40,s] A. Lath,[53] G. Latino,[47c,47a] I. Lazzizzera,[44b,44a] T. LeCompte,[2] E. Lee,[54] H. S. Lee,[14] S. W. Lee,[54,u] S. Leone,[47a] J. D. Lewis,[18] C.-S. Lin,[29] J. Linacre,[43] M. Lindgren,[18] E. Lipeles,[46] A. Lister,[8] D. O. Litvintsev,[18] C. Liu,[48] T. Liu,[18] N. S. Lockyer,[46] A. Loginov,[61] M. Loreti,[44b,44a] L. Lovas,[15] D. Lucchesi,[44b,44a] C. Luci,[52b,52a] J. Lueck,[27] P. Lujan,[29] P. Lukens,[18] G. Lungu,[51] L. Lyons,[43] J. Lys,[29] R. Lysak,[15] D. MacQueen,[34] R. Madrak,[18] K. Maeshima,[18] K. Makhoul,[33] T. Maki,[24] P. Maksimovic,[26] S. Malde,[43] S. Malik,[31] G. Manca,[30,f] A. Manousakis-Katsikakis,[3] F. Margaroli,[49] C. Marino,[27] C. P. Marino,[25] A. Martin,[61] V. Martin,[22,l] M. Martínez,[4] R. Martínez-Ballarín,[32] T. Maruyama,[56] P. Mastrandrea,[52a] T. Masubuchi,[56] M. Mathis,[26] M. E. Mattson,[59] P. Mazzanti,[6a] K. S. McFarland,[50] P. McIntyre,[54] R. McNulty,[30,k] A. Mehta,[30] P. Mehtala,[24] A. Menzione,[47a] P. Merkel,[49] C. Mesropian,[51] T. Miao,[18] N. Miladinovic,[7] R. Miller,[36] C. Mills,[23] M. Milnik,[27] A. Mitra,[1] G. Mitselmakher,[19] H. Miyake,[56] N. Moggi,[6a] C. S. Moon,[28] R. Moore,[18] M. J. Morello,[47b,47a] J. Morlock,[27] P. Movilla Fernandez,[18] J. Mülmenstädt,[29] A. Mukherjee,[18] Th. Muller,[27] R. Mumford,[26] P. Murat,[18] M. Mussini,[6b,6a] J. Nachtman,[18] Y. Nagai,[56] A. Nagano,[56] J. Naganoma,[56] K. Nakamura,[56] I. Nakano,[41] A. Napier,[57] V. Necula,[17] J. Nett,[60]

C. Neu,[46,w] M. S. Neubauer,[25] S. Neubauer,[27] J. Nielsen,[29,h] L. Nodulman,[2] M. Norman,[10] O. Norniella,[25] E. Nurse,[31] L. Oakes,[43] S. H. Oh,[17] Y. D. Oh,[28] I. Oksuzian,[19] T. Okusawa,[42] R. Orava,[24] K. Osterberg,[24] S. Pagan Griso,[44b,44a] E. Palencia,[18] V. Papadimitriou,[18] A. Papaikonomou,[27] A. A. Paramonov,[14] B. Parks,[40] S. Pashapour,[34] J. Patrick,[18] G. Pauletta,[55b,55a] M. Paulini,[13] C. Paus,[33] T. Peiffer,[27] D. E. Pellett,[8] A. Penzo,[55a] T. J. Phillips,[17] G. Piacentino,[47a] E. Pianori,[46] L. Pinera,[19] K. Pitts,[25] C. Plager,[9] L. Pondrom,[60] O. Poukhov,[16,a] N. Pounder,[43] F. Prakoshyn,[16] A. Pronko,[18] J. Proudfoot,[2] F. Ptohos,[18,j] E. Pueschel,[13] G. Punzi,[47b,47a] J. Pursley,[60] J. Rademacker,[43,d] A. Rahaman,[48] V. Ramakrishnan,[60] N. Ranjan,[49] I. Redondo,[32] P. Renton,[43] M. Renz,[27] M. Rescigno,[52a] S. Richter,[27] F. Rimondi,[6b,6a] L. Ristori,[47a] A. Robson,[22] T. Rodrigo,[12] T. Rodriguez,[46] E. Rogers,[25] S. Rolli,[57] R. Roser,[18] M. Rossi,[55a] R. Rossin,[11] P. Roy,[34] A. Ruiz,[12] J. Russ,[13] V. Rusu,[18] B. Rutherford,[18] H. Saarikko,[24] A. Safonov,[54] W. K. Sakumoto,[50] O. Saltó,[4] L. Santi,[55b,55a] S. Sarkar,[52b,52a] L. Sartori,[47a] K. Sato,[18] A. Savoy-Navarro,[45] P. Schlabach,[18] A. Schmidt,[27] E. E. Schmidt,[18] M. A. Schmidt,[14] M. P. Schmidt,[61,a] M. Schmitt,[39] T. Schwarz,[8] L. Scodellaro,[12] A. Scribano,[47c,47a] F. Scuri,[47a] A. Sedov,[49] S. Seidel,[38] Y. Seiya,[42] A. Semenov,[16] L. Sexton-Kennedy,[18] F. Sforza,[47a] A. Sfyrla,[25] S. Z. Shalhout,[59] T. Shears,[30] P. F. Shepard,[48] M. Shimojima,[56,r] S. Shiraishi,[14] M. Shochet,[14] Y. Shon,[60] I. Shreyber,[37] A. Sidoti,[47a] P. Sinervo,[34] A. Sisakyan,[16] A. J. Slaughter,[18] J. Slaunwhite,[40] K. Sliwa,[57] J. R. Smith,[8] F. D. Snider,[18] R. Snihur,[34] A. Soha,[8] S. Somalwar,[53] V. Sorin,[36] J. Spalding,[18] T. Spreitzer,[34] P. Squillacioti,[47c,47a] M. Stanitzki,[61] R. St. Denis,[22] B. Stelzer,[34] O. Stelzer-Chilton,[34] D. Stentz,[39] J. Strologas,[38] G. L. Strycker,[35] D. Stuart,[11] J. S. Suh,[28] A. Sukhanov,[19] I. Suslov,[16] T. Suzuki,[56] A. Taffard,[25,g] R. Takashima,[41] Y. Takeuchi,[56] R. Tanaka,[41] M. Tecchio,[35] P. K. Teng,[1] K. Terashi,[51] J. Thom,[18,i] A. S. Thompson,[22] G. A. Thompson,[25] E. Thomson,[46] P. Tipton,[61] P. Ttito-Guzmán,[32] S. Tkaczyk,[18] D. Toback,[54] S. Tokar,[15] K. Tollefson,[36] T. Tomura,[56] D. Tonelli,[18] S. Torre,[20] D. Torretta,[18] P. Totaro,[55b,55a] S. Tourneur,[45] M. Trovato,[47a] S.-Y. Tsai,[1] Y. Tu,[46] N. Turini,[47c,47a] F. Ukegawa,[56] S. Vallecorsa,[21] N. van Remortel,[24,c] A. Varganov,[35] E. Vataga,[47d,47a] F. Vázquez,[19,o] G. Velev,[18] C. Vellidis,[3] M. Vidal,[32] R. Vidal,[18] I. Vila,[12] R. Vilar,[12] T. Vine,[31] M. Vogel,[38] I. Volobouev,[29,u] G. Volpi,[47b,47a] P. Wagner,[46] R. G. Wagner,[2] R. L. Wagner,[18] W. Wagner,[27,x] J. Wagner-Kuhr,[27] T. Wakisaka,[42] R. Wallny,[9] S. M. Wang,[1] A. Warburton,[34] D. Waters,[31] M. Weinberger,[54] J. Weinelt,[27] W. C. Wester III,[18] B. Whitehouse,[57] D. Whiteson,[46,g] A. B. Wicklund,[2] E. Wicklund,[18] S. Wilbur,[14] G. Williams,[34] H. H. Williams,[46] P. Wilson,[18] B. L. Winer,[40] P. Wittich,[18,i] S. Wolbers,[18] C. Wolfe,[14] T. Wright,[35] X. Wu,[21] F. Würthwein,[10] S. Xie,[33] A. Yagil,[10] K. Yamamoto,[42] J. Yamaoka,[17] U. K. Yang,[14,q] Y. C. Yang,[28] W. M. Yao,[29] G. P. Yeh,[18] J. Yoh,[18] K. Yorita,[58] T. Yoshida,[42,n] G. B. Yu,[50] I. Yu,[28] S. S. Yu,[18] J. C. Yun,[18] L. Zanello,[52b,52a] A. Zanetti,[55a] X. Zhang,[25] Y. Zheng,[9,e] and S. Zucchelli[6b,6a]

(CDF Collaboration)

[1]*Institute of Physics, Academia Sinica, Taipei, Taiwan 11529, Republic of China*
[2]*Argonne National Laboratory, Argonne, Illinois 60439*
[3]*University of Athens, 157 71 Athens, Greece*
[4]*Institut de Fisica d'Altes Energies, Universitat Autonoma de Barcelona, E-08193, Bellaterra (Barcelona), Spain*
[5]*Baylor University, Waco, Texas 76798, USA*
[6a]*Istituto Nazionale di Fisica Nucleare Bologna, I-40127 Bologna, Italy*
[6b]*University of Bologna, I-40127 Bologna, Italy*
[7]*Brandeis University, Waltham, Massachusetts 02254, USA*
[8]*University of California, Davis, Davis, California 95616, USA*
[9]*University of California, Los Angeles, Los Angeles, California 90024, USA*
[10]*University of California, San Diego, La Jolla, California 92093, USA*
[11]*University of California, Santa Barbara, Santa Barbara, California 93106, USA*
[12]*Instituto de Fisica de Cantabria, CSIC-University of Cantabria, 39005 Santander, Spain*
[13]*Carnegie Mellon University, Pittsburgh, Pennsylvania 15213, USA*
[14]*Enrico Fermi Institute, University of Chicago, Chicago, Illinois 60637, USA*
[15]*Comenius University, 842 48 Bratislava, Slovakia; Institute of Experimental Physics, 040 01 Kosice, Slovakia*
[16]*Joint Institute for Nuclear Research, RU-141980 Dubna, Russia*
[17]*Duke University, Durham, North Carolina 27708, USA*
[18]*Fermi National Accelerator Laboratory, Batavia, Illinois 60510, USA*
[19]*University of Florida, Gainesville, Florida 32611, USA*
[20]*Laboratori Nazionali di Frascati, Istituto Nazionale di Fisica Nucleare, I-00044 Frascati, Italy*
[21]*University of Geneva, CH-1211 Geneva 4, Switzerland*
[22]*Glasgow University, Glasgow G12 8QQ, United Kingdom*
[23]*Harvard University, Cambridge, Massachusetts 02138, USA*

[24]*Division of High Energy Physics, Department of Physics, University of Helsinki and Helsinki Institute of Physics, FIN-00014, Helsinki, Finland*
[25]*University of Illinois, Urbana, Illinois 61801, USA*
[26]*The Johns Hopkins University, Baltimore, Maryland 21218, USA*
[27]*Institut für Experimentelle Kernphysik, Universität Karlsruhe, 76128 Karlsruhe, Germany*
[28]*Center for High Energy Physics: Kyungpook National University, Daegu 702-701, Korea; Seoul National University, Seoul 151-742, Korea; Sungkyunkwan University, Suwon 440-746, Korea; Korea Institute of Science and Technology Information, Daejeon, 305-806, Korea; Chonnam National University, Gwangju, 500-757, Korea*
[29]*Ernest Orlando Lawrence Berkeley National Laboratory, Berkeley, California 94720, USA*
[30]*University of Liverpool, Liverpool L69 7ZE, United Kingdom*
[31]*University College London, London WC1E 6BT, United Kingdom*
[32]*Centro de Investigaciones Energeticas Medioambientales y Tecnologicas, E-28040 Madrid, Spain*
[33]*Massachusetts Institute of Technology, Cambridge, Massachusetts 02139, USA*
[34]*Institute of Particle Physics: McGill University, Montréal, Québec, Canada H3A 2T8; Simon Fraser University, Burnaby, British Columbia, Canada V5A 1S6; University of Toronto, Toronto, Ontario, Canada M5S 1A7; and TRIUMF, Vancouver, British Columbia, Canada V6T 2A3*
[35]*University of Michigan, Ann Arbor, Michigan 48109, USA*
[36]*Michigan State University, East Lansing, Michigan 48824, USA*
[37]*Institution for Theoretical and Experimental Physics, ITEP, Moscow 117259, Russia*
[38]*University of New Mexico, Albuquerque, New Mexico 87131, USA*
[39]*Northwestern University, Evanston, Illinois 60208, USA*
[40]*The Ohio State University, Columbus, Ohio 43210, USA*
[41]*Okayama University, Okayama 700-8530, Japan*
[42]*Osaka City University, Osaka 588, Japan*
[43]*University of Oxford, Oxford OX1 3RH, United Kingdom*
[44a]*Istituto Nazionale di Fisica Nucleare, Sezione di Padova-Trento, I-35131 Padova, Italy*
[44b]*University of Padova, I-35131 Padova, Italy*
[45]*LPNHE, Universite Pierre et Marie Curie/IN_2P_3-CNRS, UMR7585, Paris, F-75252 France*
[46]*University of Pennsylvania, Philadelphia, Pennsylvania 19104, USA*
[47a]*Istituto Nazionale di Fisica Nucleare Pisa, I-56127 Pisa, Italy*
[47b]*University of Pisa, I-56127 Pisa, Italy*
[47c]*University of Siena, I-56127 Pisa, Italy*
[47d]*Scuola Normale Superiore, I-56127 Pisa, Italy*
[48]*University of Pittsburgh, Pittsburgh, Pennsylvania 15260, USA*
[49]*Purdue University, West Lafayette, Indiana 47907, USA*

[a]Deceased.
[b]Visitor from University of Massachusetts Amherst, Amherst, MA 01003, USA.
[c]Visitor from Universiteit Antwerpen, B-2610 Antwerp, Belgium.
[d]Visitor from University of Bristol, Bristol BS8 1TL, United Kingdom.
[e]Visitor from Chinese Academy of Sciences, Beijing 100864, China.
[f]Visitor from Istituto Nazionale di Fisica Nucleare, Sezione di Cagliari, 09042 Monserrato (Cagliari), Italy.
[g]Visitor from University of California Irvine, Irvine, CA 92697, USA.
[h]Visitor from University of California Santa Cruz, Santa Cruz, CA 95064, USA.
[i]Visitor from Cornell University, Ithaca, NY 14853, USA.
[j]Visitor from University of Cyprus, Nicosia CY-1678, Cyprus.
[k]Visitor from University College Dublin, Dublin 4, Ireland.
[l]Visitor from University of Edinburgh, Edinburgh EH9 3JZ, United Kingdom.
[m]Visitor from University of Fukui, Fukui City, Fukui Prefecture, Japan 910-0017.
[n]Visitor from Kinki University, Higashi-Osaka City, Japan 577-8502.
[o]Visitor from Universidad Iberoamericana, Mexico D.F., Mexico.
[p]Visitor from Queen Mary, University of London, London, E1 4NS, England.
[q]Visitor from University of Manchester, Manchester M13 9PL, England.
[r]Visitor from Nagasaki Institute of Applied Science, Nagasaki, Japan.
[s]Visitor from University of Notre Dame, Notre Dame, IN 46556, USA.
[t]Visitor from University de Oviedo, E-33007 Oviedo, Spain.
[u]Visitor from Texas Tech University, Lubbock, TX 79609, USA.
[v]Visitor from IFIC(CSIC-Universitat de Valencia), 46071 Valencia, Spain.
[w]Visitor from University of Virginia, Charlottesville, VA 22904, USA.
[x]Visitor from Bergische Universität Wuppertal, 42097 Wuppertal, Germany.
[y]On leave from J. Stefan Institute, Ljubljana, Slovenia.

[50]*University of Rochester, Rochester, New York 14627, USA*
[51]*The Rockefeller University, New York, New York 10021, USA*
[52a]*Istituto Nazionale di Fisica Nucleare, Sezione di Roma 1, I-00185 Roma, Italy*
[52b]*Sapienza Università di Roma, I-00185 Roma, Italy*
[53]*Rutgers University, Piscataway, New Jersey 08855*
[54]*Texas A&M University, College Station, Texas 77843, USA*
[55a]*Istituto Nazionale di Fisica Nucleare Trieste/Udine, I-34100 Trieste, Italy*
[55b]*University of Trieste/Udine, I-33100 Udine, Italy*
[56]*University of Tsukuba, Tsukuba, Ibaraki 305, Japan*
[57]*Tufts University, Medford, Massachusetts 02155, USA*
[58]*Waseda University, Tokyo 169, Japan*
[59]*Wayne State University, Detroit, Michigan 48201, USA*
[60]*University of Wisconsin, Madison, Wisconsin 53706, USA*
[61]*Yale University, New Haven, Connecticut 06520, USA*
(Received 4 May 2009; published 8 September 2009)

We have used the Collider Detector at Fermilab (CDF-II) to search for the flavor-changing neutral-current (FCNC) top-quark decay $t \to Zc$ using a technique employing ratios of W and Z production, measured in $p\bar{p}$ data corresponding to an integrated luminosity of 1.52 fb^{-1}. The analysis uses a comparison of two decay chains, $p\bar{p} \to t\bar{t} \to WbWb \to \ell\nu bjjb$ and $p\bar{p} \to t\bar{t} \to ZcWb \to \ell\ell cjjb$, to cancel systematic uncertainties in acceptance, efficiency, and luminosity. We validate the modeling of acceptance and efficiency for lepton identification over the multiyear data set using another ratio of W and Z production, in this case the observed ratio of inclusive production of W to Z bosons. To improve the discrimination against standard model backgrounds to top-quark decays, we calculate the top-quark mass for each event with two leptons and four jets assuming it is a $t\bar{t}$ event with one of the top quarks decaying to Zc. For additional background discrimination we require at least one jet to be identified as originating from a b quark. No significant signal is found and we set an upper limit on the FCNC branching ratio Br($t \to Zc$) using a likelihood constructed from the $\ell\ell cjjb$ top-quark mass distribution and the number of $\ell\nu bjjb$ events. Limits are set as a function of the helicity of the Z boson produced in the FCNC decay. For 100% longitudinally-polarized Z bosons we find limits of 8.3% and 9.3% (95% C.L.) depending on the assumptions regarding the theoretical top-quark pair production cross section.

DOI: 10.1103/PhysRevD.80.052001 PACS numbers: 13.85.Rm, 12.60.Cn, 13.85.Qk, 14.65.Ha

I. INTRODUCTION

The standard model (SM) Lagrangian does not contain any flavor-changing neutral-current (FCNC) terms such as $d \to s$, a consequence of its SU(2) structure [1]. In the SM the top quark is expected to decay via the charged weak current into a W boson and a bottom quark, $t \to W^+ b$, with close to 100% branching ratio [2]. We test this prediction by searching for FCNC interactions in top-quark decays, in which the top quark decays to a Z boson and a charm quark, $t \to Zc$. In the standard model the FCNC decay $t \to Zc$ is highly suppressed, proceeding only through radiative corrections, with a predicted branching ratio Br($t \to Zc$) of about 10^{-14} [3]. However, some extensions of the SM (e.g., two-Higgs doublet models, models with extra quark singlets, technicolor models with a dynamical breakdown of the electroweak symmetry, etc.) predict measurable rates [1,4,5].

The production of top-quark pairs, $t\bar{t}$, is the preferred channel to observe the FCNC transition $t \to c$ at the Tevatron, as single top-quark production has a smaller cross section and much larger QCD backgrounds in the Zc final state. We have used data from an integrated luminosity of 1.52 fb^{-1} collected with the CDF-II detector [6] at the Fermilab Tevatron to search for events in which one of the top quarks decays to Zc and the other one decays to Wb. In order to get a sample of high purity, we select the leptonic decays of the Z boson, $Z \to e^+e^-$, and $Z \to \mu^+\mu^-$. In this scenario, the FCNC signature is most likely a pair of oppositely-charged leptons forming a Z boson, and four jets (the b and c jets from the t and $\bar{t}$, and two jets from $W \to q\bar{q}'$), with the event being kinematically consistent with the FCNC $t\bar{t}$ decay hypothesis. We require at least one jet with a displaced secondary vertex as a sign of a heavy-flavor quark (b or c quark) to further suppress hadronic backgrounds.

To minimize the systematic uncertainties on the particle identification and trigger efficiencies, geometric acceptances, and luminosity, we rely on a technique based on the simultaneous comparison of two decay chains:

(1) $p\bar{p} \to t\bar{t} \to WbWb \to \ell\nu bjjb$ (see Fig. 1),
(2) $p\bar{p} \to t\bar{t} \to ZcWb \to \ell\ell cjjb$ (see Fig. 2).

Many of the systematic uncertainties contributing to both decay chains are correlated and tend to cancel, improving the precision and robustness of the result. The other decay modes of top-quark pairs (e.g., $t\bar{t} \to WbWb \to \ell_1\nu_1 b\ell_2\nu_2 b$, $t\bar{t} \to WbWb \to jjbjjb$, or $t\bar{t} \to ZcWb \to \ell_1^+\ell_1^- c\ell_2\nu_2 b$) have low acceptances or high levels of background and are not used.

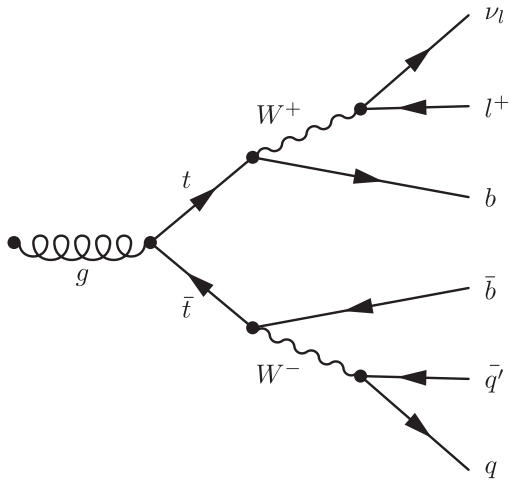

FIG. 1. A Feynman diagram for one of the processes contributing to the $p\bar{p} \to t\bar{t} \to WbWb \to \ell\nu bjjb$ decay chain.

The final states $\ell\nu bjjb$ and $\ell\ell cjjb$ used in this analysis contain products of the leptonic decays of $W \to \ell\nu$ and $Z \to \ell\ell$, for which there exist precise next-to-next-to-leading order (NNLO) predictions of inclusive cross sections multiplied by branching fractions [7]. We use a comparison of the measured ratio of inclusive $W \to \ell\nu$ to $Z \to \ell\ell$ production to validate the lepton identification and trigger efficiencies in the Monte Carlo simulation predictions of signal and SM background to about 2%. This technique, which parallels that used in the search, will be used for precision comparisons with the standard model at the LHC [8].

We present a technique for measuring the background in the inclusive W boson sample coming from QCD multijet events using a data-derived model [9,10]. The number of misidentified W bosons is estimated separately for electrons and muons by fitting the observed distributions in $\not\!\!E_{\mathrm{T}}$ [11] with templates from real W decays and modeled non-W events.

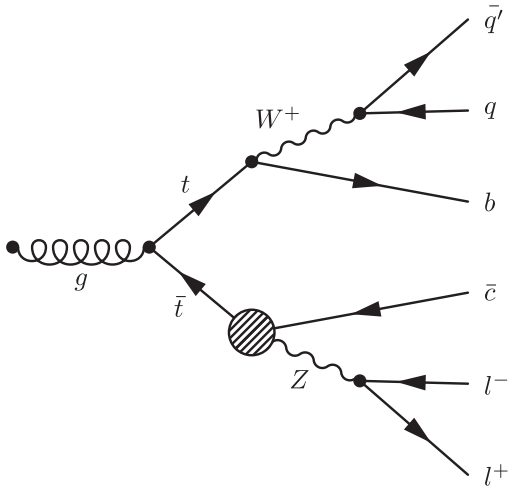

FIG. 2. A Feynman diagram for one of the processes contributing to the $p\bar{p} \to t\bar{t} \to ZcWb \to \ell\ell cjjb$ decay chain. The blob represents a non-SM FCNC vertex.

We also present a simple technique to estimate the number of muons from cosmic rays in the Z boson sample, using the distribution in the magnitude of the vector momentum sum, $|\vec{P}(\mu^+\mu^-)|$, of the muon pair. This is an economical way of combining the usual "back-to-back" and momentum balance criteria for the two muons into a single distribution, as $\mu^+\mu^-$ pairs from cosmic rays have a very narrow peak at $|\vec{P}(\mu^+\mu^-)| = 0$ GeV, while real $Z \to \mu^+\mu^-$ decays occupy a much larger volume in the 3-dimensional momentum space.

A previous limit on the branching ratio for $t \to Zc$ [2] is from CDF using data from Run I of the Tevatron; the limit is 33% at 95% confidence level (C.L.) [13]. The limit from precision measurements at LEP is lower, 13.7% at 95% C.L. [14].

There is a recent CDF limit from a parallel independent analysis, using a different technique and a total luminosity of 1.9 fb^{-1}, of 3.7% at 95% C.L., more restrictive than the result presented here [15]. The technique presented here is specifically designed to reduce systematic errors by using ratios of W and Z boson events, important for much larger integrated luminosities [8]. The acceptance for $t\bar{t} \to ZcWb \to \ell\ell cjjb$ events in this analysis is 0.303% versus the 0.43% quoted in Ref. [15].

We derive the first upper limits on $\mathrm{Br}(t \to Zc)$ as a function of the polarization of the Z boson produced in a FCNC decay of a top quark. These limits cover all possible FCNC top-quark couplings.

The outline of the paper is as follows. Section II briefly describes the CDF-II detector. The analysis strategy, which uses the SM decay modes of the top quark as well as the signal FCNC decay mode to allow cancellation of major systematic uncertainties of acceptance, efficiency, and luminosity, is described in Sec. III. Section IV describes the event selection, which starts with the data set of events selected on central [12] high transverse momentum [11] electrons and muons. The identification of jets containing heavy flavor is given in Sec. IV D. Sections V and VI describe the selection of Z and W bosons, respectively. The modeling and validation of standard model vector boson production and the estimation of backgrounds are presented in Sec. VII. Section VIII describes the technique of using the measurement of R, the ratio of inclusive W boson to inclusive Z boson production, as a check of the complex Monte Carlo samples generated using the detector and accelerator conditions accumulated over the long period of data taking. Section IX describes the modeling of the FCNC signal from top-quark decay. The measurement of the expected SM contributions to the signature W boson + 4-jets with one jet identified as heavy flavor, dominated by top-quark pair production, is described in Sec. X. The contributions to the reference channel,

W boson + 4-jets, and the signal channel, Z boson + 4-jets, each with one or more heavy-flavor jets, are presented in Secs. XI and XII, respectively.

The estimation of systematic uncertainties on the acceptances and backgrounds is described in Sec. XIII, and the limit calculations for a full range of possible longitudinal FCNC couplings are presented in Sec. XIV. Section XV is a summary of the conclusions.

II. THE CDF-II DETECTOR

The CDF-II detector is a cylindrically symmetric spectrometer designed to study $p\bar{p}$ collisions at the Fermilab Tevatron. The detector has been extensively described in the literature [6]. Here we briefly describe the detector subsystems relevant for the analysis.

Tracking systems are used to measure the momenta of charged particles, and to trigger on and identify leptons with large transverse momentum, p_T [11]. A multilayer system of silicon strip detectors [16], which identifies tracks in both the $r-\phi$ and $r-z$ views [12], and the central outer tracker (COT) [17] are contained in a superconducting solenoid that generates a magnetic field of 1.4 T. The COT is a 3.1 m long open-cell drift chamber that makes up to 96 measurements along the track of each charged particle in the region $|\eta| < 1$. Sense wires are arranged in 8 alternating axial and stereo ($\pm 2°$) superlayers with 12 wires each. For high momentum tracks, the COT p_T resolution is $\sigma_{p_T}/p_T^2 \simeq 0.0017\ \mathrm{GeV}^{-1}$ [18].

Segmented calorimeters with towers arranged in a projective geometry, each tower consisting of an electromagnetic and a hadronic compartment [19,20], cover the central region, $|\eta| < 1$ (central electromagnetic calorimeter/central hadronic calorimeter), and the "end-plug" region, $1 < |\eta| < 3.6$ (plug electromagnetic calorimeter/plug hadronic calorimeter). In both the central and end-plug regions, systems with finer spatial resolution are used to make profile measurements of electromagnetic showers at shower maximum [21] for electron identification (the central electromagnetic shower maximum detector and plug electromagnetic shower maximum detector systems, respectively). Electrons are reconstructed in the central electromagnetic calorimeter with an E_T [11] resolution of $\sigma(E_T)/E_T \simeq 13.5\%/\sqrt{E_T/\mathrm{GeV}} \oplus 2\%$ [19] and in the plug electromagnetic calorimeter with an E_T resolution of $\sigma(E_T)/E_T \simeq 16.0\%/\sqrt{E_T/\mathrm{GeV}} \oplus 1\%$ [22]. Jets are identified using a cone clustering algorithm in $\eta-\phi$ space of radius 0.4 as a group of electromagnetic and hadronic calorimeter towers; the jet-energy resolution is approximately $\sigma \simeq 0.1 \cdot E_T(\mathrm{GeV}) + 1.0\ \mathrm{GeV}$ [23].

Muons are identified using the central muon detector (CMU), central muon upgrade detector (CMP), and central muon extension detector (CMX)[24,25], which cover the kinematic region $|\eta| < 1$. The CMU system uses four layers of planar drift chambers to detect muons with $p_T > 1.4$ GeV in the central region of $|\eta| < 0.6$. The CMP system consists of an additional four layers of planar drift chambers located behind 0.6 m of steel outside the magnetic return yoke, and detects muons with $p_T > 2.0$ GeV. The CMX detects muons in the region $0.6 < |\eta| < 1.0$ with four to eight layers of drift chambers, depending on the polar angle.

The beam luminosity is measured using two sets of gas Cherenkov counters, located in the region $3.7 < |\eta| < 4.7$. The total uncertainty on the luminosity is estimated to be 5.9%, where 4.4% comes from the acceptance and operation of the luminosity monitor and 4.0% from the calculation of the inelastic $p\bar{p}$ cross section [26].

A 3-level trigger system [6] selects events for further analysis offline. The first two levels of triggers consist of dedicated fast digital electronics analyzing a subset of the full detector data. The third level, applied to the full data from the detector for those events passing the first two levels, consists of a farm of computers that reconstruct the data and apply selection criteria for (typically) several hundred distinct triggers.

III. INTRODUCTION TO THE ANALYSIS STRATEGY

The measurement of the branching ratio of the $t \to Zc$ decay mode is designed to be similar to the measurement of the R ratio between the inclusive cross section of W's to Z's. The ratio R is defined as

$$R = \frac{\sigma(W) \cdot \mathrm{Br}(W \to \ell\nu)}{\sigma(Z) \cdot \mathrm{Br}(Z \to \ell\ell)}, \tag{1}$$

where $\sigma(W)$ and $\sigma(Z)$ are cross sections of inclusively produced W and Z bosons. A measurement of the R ratio is itself a precise test of lepton identification efficiencies, triggering, and Monte Carlo simulations. A measured R ratio has smaller uncertainties than $\sigma(W)$ and $\sigma(Z)$ since some of the uncertainties (e.g., for integrated luminosity) completely cancel out. This makes R a valuable tool for precise comparisons between experimental and theoretical predictions for channels involving both W and Z bosons.

We estimate R for electrons and muons separately (see Sec. VIII) since these particles are identified with different detector subsystems. The observed numbers are consistent with the theoretical predictions [27,28] and the previous CDF measurement [29] (see Sec. VIII). This cross-check was performed before measuring the branching ratio $\mathrm{Br}(t \to Zc)$.

The measurement of $\mathrm{Br}(t \to Zc)$ is designed to be a measurement of the ratio between events in exclusive final states with a Z boson and four jets and a W boson and four jets. In the case of the FCNC scenario, a larger FCNC branching fraction leads to fewer top-quark events decaying to W + 4 jets, and consequently an increase in the rate of Z + 4 jets events. We subtract SM non-$t\bar{t}$ events from events with a W or a Z boson and four jets so that the ratio

is more sensitive to the FCNC signal. The ratio of $Z + 4$ jets to $W + 4$ jets increases in presence of FCNC events.

IV. EVENT SELECTION

The analysis uses events selected by the trigger system that contain either a central electron with $E_T > 18$ GeV or a muon with $p_T > 18$ GeV [11]. The electron data set contains 75.5 M events; the muon data set contains about 21.2 M events. The integrated luminosity of each data set is 1.52 fb^{-1}.

Both the observed and the simulated events (see Sec. VII A) are processed through the same selection criteria to identify electrons and muons, jets, W and Z bosons, missing transverse energy, and jets containing heavy flavor. Details of the selection criteria are provided below.

A. Lepton identification

We use standard CDF definitions for identification (ID) of electrons and muons, as described below [29]. The same lepton ID requirements are applied to events from data and Monte Carlo simulations.

The identification and triggering efficiencies for leptons are different for events in data and Monte Carlo (MC), although they demonstrate a very similar energy dependence. To eliminate this inconsistency, we follow the standard CDF practice of using correction factors (''scale factors'') to reweight the MC events (see Sec. IV A 3).

In order to maintain a high efficiency for Z bosons, for which we require two identified leptons, we define ''tight'' and ''loose'' selection criteria for both electrons and muons, as described below.

To reduce backgrounds from the decays of hadrons produced in jets, leptons are required to be ''isolated.'' The E_T deposited in the calorimeter towers in a cone in $\eta - \varphi$ space [12] of radius $R = 0.4$ around the lepton position is summed, and the E_T due to the lepton is subtracted. The remaining E_T is required to be less than 10% of the lepton E_T for electrons or p_T for muons.

1. Electron selection

An electron candidate passing the tight selection must be central with $E_T > 20$ GeV, and have: (a) a high quality track [30] with $p_T > 0.5 \cdot E_T$ or $p_T > 50$ GeV; (b) a good transverse shower profile at shower maximum that matches the extrapolated track position; (c) a lateral sharing of energy in the two calorimeter towers containing the electron shower consistent with that expected; and (d) minimal leakage into the hadron calorimeter [31].

Additional central electrons, classified as loose electrons, are required to have $E_T > 12$ GeV and to satisfy the tight central electron criteria but with a track requirement of $p_T > 10$ GeV (rather than $0.5 \cdot E_T$), and no requirement on a shower maximum measurement or lateral energy sharing between calorimeter towers. Electrons in the end-plug calorimeters ($1.2 < |\eta| < 2.5$), also classified as loose electrons, are required to have $E_T > 12$ GeV, minimal leakage into the hadron calorimeter, a track containing at least 3 hits in the silicon tracking system, and a shower transverse shape consistent with that expected, with a centroid close to the extrapolated position of the track [32].

2. Muon selection

A muon candidate passing the tight cuts must have: (a) a well measured track in the COT [33] with $p_T > 20$ GeV; (b) energy deposited in the calorimeter consistent with expectations [34]; (c) a muon stub [35] in both the CMU and CMP, or in the CMX, consistent with the extrapolated COT track [36]; and (d) a COT track fit consistent with an outgoing particle from a $p\bar{p}$ collision and not from an incoming cosmic ray [37].

Additional muons, classified as loose, are required to have $p_T > 12$ GeV and to satisfy the same criteria as for tight muons but with relaxed COT track quality requirements. Alternatively, for muons outside the muon system fiducial volume, a loose muon must satisfy the tight muon criteria and an additional more stringent requirement on track quality, but the requirement that there be a matching stub in the muon systems is dropped.

3. Corrections due to modeling of electrons and muons in the MC events

Following the standard treatment of lepton efficiencies in CDF, we reweight Monte Carlo events to take into account the difference between the identification efficiencies measured in leptonic Z decays and those used in simulation [38]. We then make additional corrections for the difference in trigger efficiencies in simulated events and measured in data. Corrections to trigger efficiencies are typically 4% for trigger electrons, 8% for trigger muons that traverse both the CMU and CMP systems, and 5% for muons in the CMX system. The average weight for $Z \rightarrow e^+e^-$ events is 0.939; for $Z \rightarrow \mu^+\mu^-$ events it is 0.891.

B. Jet identification

Jets are reconstructed using the standard CDF cone-based clustering algorithm with a cone radius of $R = 0.4$ within $|\eta| < 2.4$ [39]. The jet energies are corrected for the η-dependent response of the calorimeters and for the luminosity-dependent effect of multiple-$p\bar{p}$ interactions. The simulated calorimeter response for individual hadrons is tuned to match that in data [40]. The raw energy of the jets must be greater than 8 GeV and the corrected energy is required to be greater than 15 GeV. Jets that coincide with an identified electron or photon are removed; i.e., each calorimeter cluster can be associated with either a jet, an

electron, or a photon, which have mutually exclusive definitions to avoid any ambiguities.

There is one case for which the jet energies are corrected to the parton level rather than to the hadron level. This is done to calculate the top-quark mass in events with a Z boson and four jets (see Sec. XII).

High-p_T photons are not rare in hard-scattering events. Identifying photons as jets and then correcting them as jets can lead to misreconstructed missing transverse energy and other kinematic variables, and can be important in an analysis leading to small signal samples, as in this analysis. Photon candidates are required to have no matching track with $p_T > 1$ GeV, and at most one track with $p_T < 1$ GeV, pointing at the calorimeter cluster, good profiles in both transverse dimensions at shower maximum, and minimal leakage into the hadron calorimeter [31]. We require photons to be isolated in a slightly more restrictive fashion than that for the leptons: the sum of the p_T of all tracks in the cone must be less than $2.0\ \text{GeV} + 0.005 \times E_T$.

C. Reconstruction of missing transverse energy

Missing transverse energy ($\not\!\!E_T$) is the negative 2-dimensional vector sum of $\vec{E}_T$ of all identified objects in the event: electrons, muons, photons, jets, and unclustered energy. The unclustered energy is calculated as a 2-dimensional vector of raw calorimeter energy corrected for the energy deposited by identified jets, electrons, muons, and photons.

D. Tagging of heavy-flavor jets

We identify decays of bottom and charm quarks (heavy flavor, HF) with an algorithm that identifies displaced secondary vertices within a jet. The primary vertex is identified by fitting all prompt tracks in the event to a vertex constrained to lie on the beamline. Jets with $E_T > 15$ GeV are checked for good quality tracks with hits in the COT and the silicon detector. At least two good tracks consistent with a common vertex are required to form a secondary vertex candidate. The distance is calculated between the primary vertex and the secondary vertex candidate and projected on the jet direction. The jet is considered to contain a HF quark (''b tagged'') if the significance of this distance is greater than 7.5σ. The algorithm has an efficiency of approximately 50% to tag a b jet, depending on the E_T of the jet, in a $t\bar{t}$ event. More details of the algorithm are available in [41].

To model the multiple SM sources of tagged events, we use control samples selected from the data to estimate mistag rates (i.e., the fraction of tags coming from non-HF jets), and Monte Carlo simulated samples to get the contribution from SM physics processes with true heavy-flavor jets.

The contribution from real HF jets is estimated by applying the tagging algorithm to Z + HF and W + HF MC samples. Events with at least one b tag are selected. Each selected event is reweighted by $(1 - (1 - \epsilon_{\text{tag}})^{N_{\text{tags}}})$ using the per-tagged-jet scale factor $\epsilon_{\text{tag}} = 0.95 \pm 0.05$ [41,42], where N_{tags} is the number of b-tagged jets in the event, to take into account the difference in the tagging efficiencies between data and simulation.

The mistag rate is estimated by applying the mistag parametrization [42] to each event in a data sample that has all the desired characteristics except a b tag (called the ''pretag'' sample). The parametrization gives each jet a probability to be falsely tagged based on the jet E_T, η, and number of tracks of good quality in the jet.

The calculation of the mistag rate is performed in three steps. First we select all jets with $E_T > 10$ GeV and $|\eta| < 2.4$ in the event. We then apply the mistag parameterization to the selected jets. Finally we loop through jets satisfying the event selection requirements (see Sec. IV B) to calculate the probability for each jet to be falsely tagged as originating from a decay of a bottom or charm quark. The per jet mistag probability is roughly 1%.

V. PRODUCTION OF Z BOSONS WITH JETS

To be identified as a Z boson, a pair of opposite-sign electrons or muons must have a reconstructed invariant mass in the mass window from 66 to 116 GeV. The selection of $Z \to \ell\ell$ events requires two tight leptons or a tight and a loose lepton. The two leptons are required to be assigned the same primary vertex. Figure 3 shows the distributions in invariant mass for electron and muon pairs.

The SM expectation for events with a Z boson and jets is constructed using Monte Carlo simulations of SM electroweak processes such as production of WW, WZ, ZZ, and $Z \to \tau\tau$ (see Sec. VII).

The detection of Z bosons is less sensitive to the lepton trigger efficiencies than the detection of W bosons, since there are two leptons in each Z event.

VI. PRODUCTION OF W BOSONS WITH JETS

The selection of $W \to \ell\nu$ events requires a tight central electron or a tight muon and $\not\!\!E_T$ greater than 25 GeV. We require that each W event has only one tight lepton and no loose leptons. The transverse mass [43], $M_{\text{trans}}(\ell\nu)$, reconstructed from the lepton and the missing transverse energy is required to be greater than 20 GeV. Figure 4 shows the measured and expected distributions in transverse mass for the $W \to e\nu$ and $W \to \mu\nu$ events.

The SM backgrounds to events with W + jets (where $W \to \ell\nu$) are estimated using the data and from MC simulations. The MC simulations are used to predict well-understood SM electroweak processes, such as $Z \to \ell\ell$, WW, WZ, and ZZ. Backgrounds that are largely instrumental, such as the misidentification of a QCD jet as a

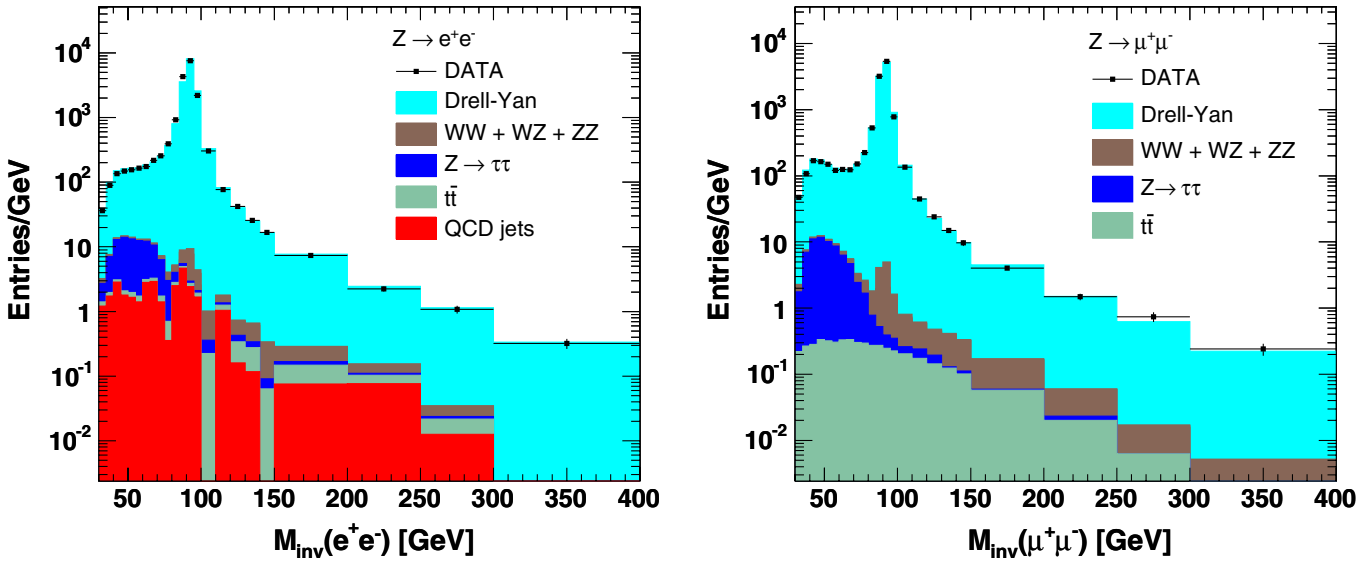

FIG. 3 (color online). The observed (points) and expected (histogram) distributions in the invariant mass of e^+e^- (left figure) and $\mu^+\mu^-$ (right figure) lepton pairs. The order of stacking in the histograms is the same as in their legends.

lepton from W decay, are predicted from the data. More details are provided in Sec. VII.

VII. STANDARD MODEL CONTRIBUTIONS TO EVENTS WITH A W OR A Z BOSON AND JETS

A. Monte Carlo simulations of the standard model processes

The standard model expectations for the production of W and Z bosons are calculated from Monte Carlo simulations. We use PYTHIA to generate W + light jets and Z + light jets processes and ALPGEN for generation of the heavy-flavor processes W + HF jets and Z + HF jets.

The data sets for the W and Z + light jets signatures are produced using a customized version of PYTHIA in which the p_T spectrum of the Z bosons, p_T^Z, has been tuned to CDF Run I data for $0 < p_T^Z < 20$ GeV, and which incorporates a tuned underlying event [44] and a requirement that $M_{\text{inv}}(\ell\ell) > 30$ GeV. The W and Z + heavy flavor jets samples are produced with a version of ALPGEN that has built-in matching of the number of jets from showering and matrix-element production [45]. Showering and hadronization of jets is done with PYTHIA [46]. Events from the MC generators, ALPGEN and PYTHIA, are processed through the full detector simulation to be reconstructed and analyzed like data.

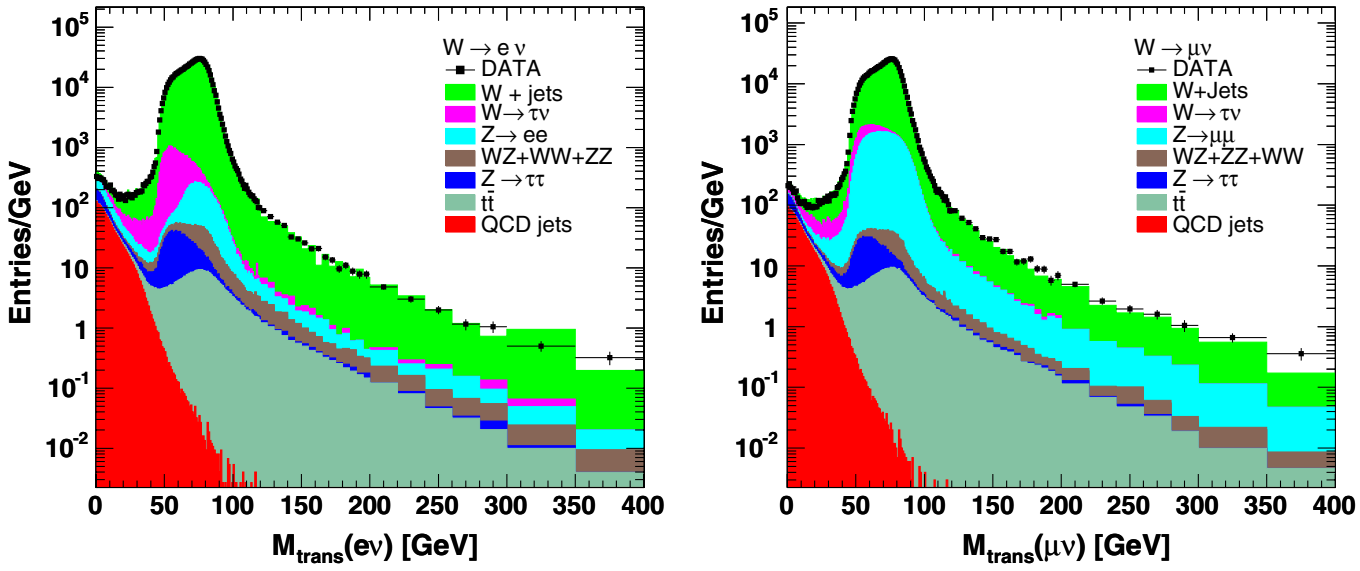

FIG. 4 (color online). The observed (points) and expected (histogram) distributions in transverse mass of $e + \not{E}_T$ (left figure) and $\mu + \not{E}_T$ (right figure). The contribution from $t\bar{t}$ production is calculated for the case when the top quarks are decaying in the standard way. The order of stacking in the histograms is the same as in their legends.

We use the CDF version of PYTHIA to describe the inclusive (i.e., before b tagging) production of W and Z bosons, used for background calculations. We use primarily ALPGEN samples to analyze b-tagged events, as PYTHIA does not handle heavy-flavor production correctly. ALPGEN handles radiation of additional jets better than PYTHIA. The inclusive production of W and Z bosons has only a second-order dependence on the difference in the jet radiation of ALPGEN and PYTHIA. It has a stronger dependence on the momentum distribution of the bosons which was tuned in the CDF version of PYTHIA as described above.

The MC contributions from the SM leading order processes are combined into inclusive samples using weights proportional to the cross sections of each contribution. These summed MC samples are then compared to the observed events in the electron and muon decay modes of W and Z bosons separately. We use NNLO cross sections of 2.687 nb and 251.3 pb for the production of W and Z bosons, respectively [29].

B. Electroweak backgrounds

Several SM processes other than Drell-Yan production of W's and Z's contribute to the W and Z leptonic signatures we use in the analysis, in particular $Z \to \tau^+\tau^-$, WW, WZ, ZZ, $W \to \tau\nu$, and $t\bar{t} \to WbWb$. These processes are estimated from corresponding MC samples, generated using PYTHIA. We weight WW, WZ, and ZZ data sets using NLO cross sections (13.0 pb, 3.96 pb, and 1.56 pb, respectively [49]).

C. Fake Z background from jets misidentified as leptons

This background consists of events in which one or more leptons are "fake," i.e., jets misidentified as leptons. We assume that in the samples with a vector boson and two-or-more jets, the true lepton and the fake lepton making up the Z in the background events have no charge correlation. As the number of fake Z bosons is small (see below), we use the number of same-sign lepton pairs to estimate the QCD jet background in the $\gamma^*/Z \to \ell\ell$ sample.

The $Z \to \mu^+\mu^-$ sample, which requires $66\ \text{GeV} < M_{\text{inv}}(\ell\ell) < 116\ \text{GeV}$, contains only 8 events with muons of the same sign out of 53 358 total events in the sample. The fake muon background is consequently negligibly small.

Same-sign electron pairs have a significant source from e^+e^- pair production by photon conversions. The observed number of same-sign electron pairs in the $Z \to e^+e^-$ sample is corrected for the predicted number of e^+e^- pairs misreconstructed as e^+e^+ or e^-e^- using MC predictions for $Z \to e^+e^-$ production.

We observe 398 same-sign electron pairs and $82\,901 e^+e^-$ pairs. We remove the contribution of real $\gamma^*/Z \to e^+e^-$ events from the number of observed events by subtracting the number of observed e^+e^- events scaled by the fraction of same-sign to opposite-sign events in the Monte Carlo samples for $Z \to e^+e^-$. The remaining 78 same-sign electron pairs are used to estimate the QCD jet background in the $Z \to e^+e^-$ sample (see Fig. 3).

D. Non-W backgrounds from jets

Jet production, which has a much higher cross section than W or Z boson production, produces events which mimic the leptonic decay of a W boson by a mismeasured jet "faking" a tight isolated lepton and large missing energy ($\not\!\!E_{\text{T}}$).

To estimate the non-W background coming from jets we use a data-derived model for non-W events. The number of misidentified W bosons (non-W) is estimated separately for electrons and muons by fitting the observed distributions in $\not\!\!E_{\text{T}}$ with templates from real W decays and modeled non-W events. The distributions in $\not\!\!E_{\text{T}}$ are fitted over the range $0 < \not\!\!E_{\text{T}} < 60$ GeV using events that contain one tight lepton and no other leptons, with transverse mass $M_{\text{trans}}(\ell\nu) > 20$ GeV (see Fig. 5). For each jet multiplicity, the non-W and the sum of the SM contributions are separately normalized in the fit to the $\not\!\!E_{\text{T}}$ distribution. The non-W events are modeled by taking electrons which pass all the selection criteria except those on the quality of the calorimeter shower (labeled "anti-selected electrons" in Fig. 5). The fractions of non-W events are estimated separately for events with 0, 1, 2, 3, and ≥ 4 jets in the final state by propagating the distribution of the modeled non-W events into the region with $\not\!\!E_{\text{T}} > 25$ GeV. The estimated fractions of non-W events for each jet multiplicity are summarized in Table I.

A systematic uncertainty of 26% is assigned on the fractions of non-W events [9], derived from the level of agreement between the shape of the data-derived non-W sample and the shape of $\not\!\!E_{\text{T}}$ distribution of misidentified electrons in data.

E. Cosmic-ray backgrounds

High-energy cosmic muons traverse the CDF detector at a significant rate and, if they intersect the beamline, can be reconstructed as $\mu^+\mu^-$ pairs. We remove cosmic-ray events with an algorithm which fits the two tracks of the $\mu^+\mu^-$ pair to a single arc composed of an incoming track segment and an outgoing segment, consistent in time evolution with a through-going track [37]. The algorithm also removes cosmic rays from events where only one muon is reconstructed as a $W \to \mu\not\!\!E_{\text{T}}$ decay. It searches for hits in the COT chamber within a narrow road along a predicted trajectory opposite to the identified muon. Finally, the algorithm performs a simultaneous fit of the hits of the muon track and the hits in the predicted trajectory with a single helix to determine consistency with the cosmic-ray hypothesis.

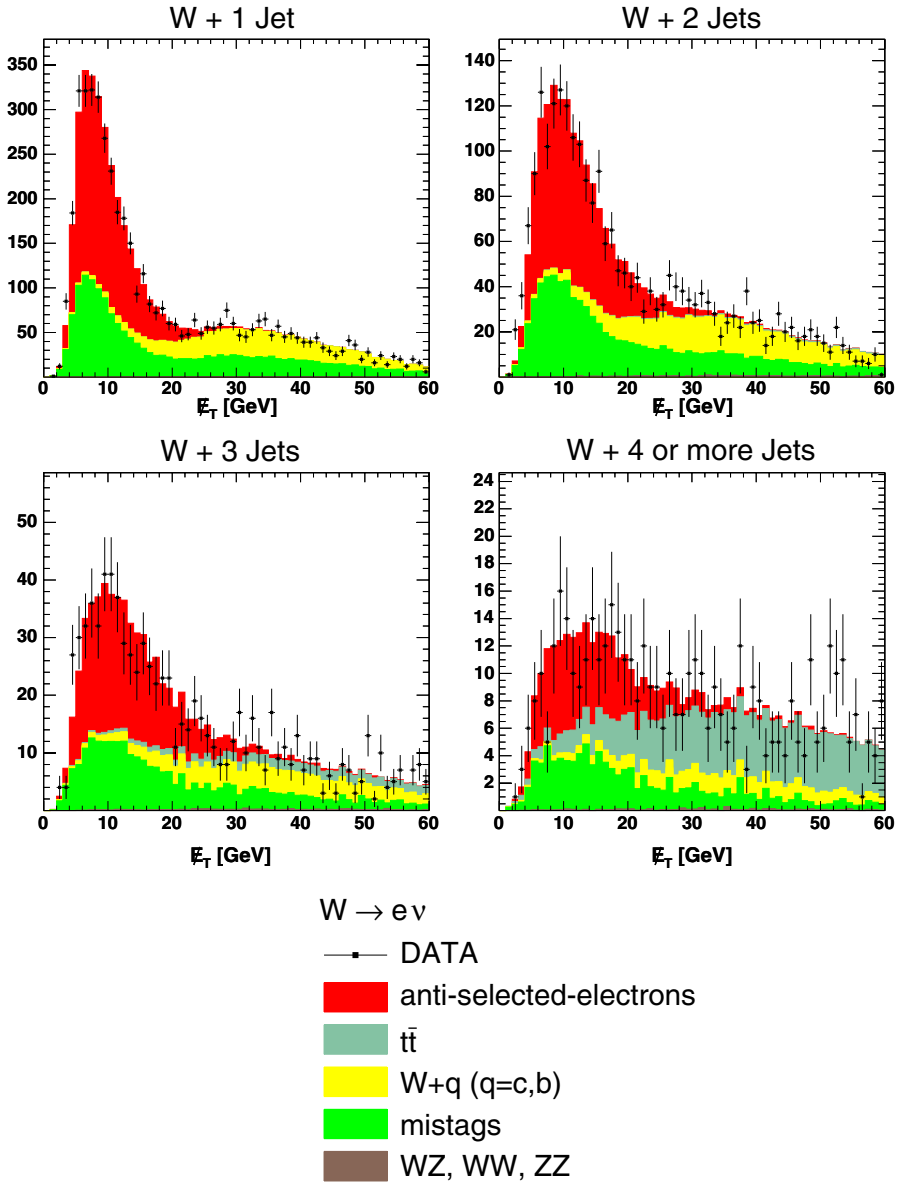

FIG. 5 (color online). The measured distribution in $\not\!\!E_T$ for events with 1, 2, 3, and 4 or more jets in events with a single tight electron and missing energy forming a transverse mass, M_{trans}, greater than 20 GeV. At least one of the jets is required to be originating from a heavy-flavor quark. The observed distributions are compared to those from SM expectations and non-W events (labeled "anti-selected electron"; see text) in order to estimate the QCD background. The order of stacking in the histograms is the same as in the legend.

TABLE I. Fractions of non-W events in events with one tight lepton and no other leptons (inclusive W), and with $\not\!\!E_T >$ 25 GeV and $M_{\text{trans}}(\ell + \not\!\!E_T) > 20$ GeV. Note that this sample is selected without the requirement of the presence of a heavy-flavor jet.

Jet Multiplicity	0 jets	1 jet	2 jets	3 jets	≥ 4 jets
$W \rightarrow e\nu +$ jets	0.6%	1.9%	7%	14%	20%
$W \rightarrow \mu\nu +$ jets	0.1%	0.3%	0.9%	1.8%	2.6%

An independent estimate of the number of cosmic muons in the Z boson sample that have survived the cosmic-ray filter can be made from the distribution of the magnitude of the momentum vector of the $\mu^+\mu^-$ pair, $|\vec{P}(\mu^+\mu^-)|$. This is a simple way of combining the usual "back-to-back" and momentum balance criteria for the two muons into a single distribution, as cosmic $\mu^+\mu^-$ pairs have a very narrow peak at $|\vec{P}(\mu^+\mu^-)| = 0$ GeV, while real $Z \rightarrow \mu^+\mu^-$ decays occupy only a small area in the 3-dimensional momentum phase space near $|\vec{P}(\mu^+\mu^-)| = 0$. Using the $|\vec{P}(\mu^+\mu^-)|$ distribution as an estimator, the number of cosmic-ray events in the

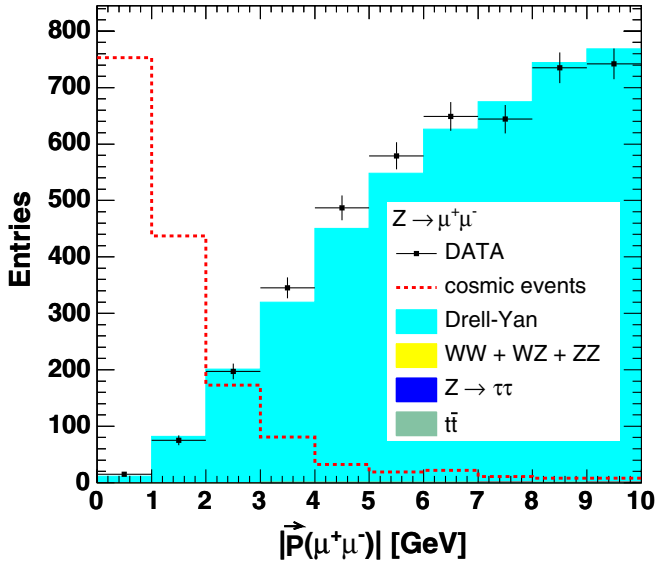

FIG. 6 (color online). The distribution $|\vec{P}(\mu^+\mu^-)|$ of muon pairs from Z boson candidates (solid lines), events expected from simulations (stacked histogram), and from a cosmic-ray sample (dashed line). The stacked histogram is mostly Drell-Yan production; the other sources are considered but have negligible contribution to the histogram. The number of cosmic-ray events in the search sample is negligible.

sample surviving the cosmic filter is negligible, as shown in Fig. 6.

VIII. USING R AS A PRECISE CHECK OF THE MONTE CARLO SIMULATIONS

The Monte Carlo simulation of a data set extending over years, with changing detector and accelerator conditions, is an exceptionally complex task, involving large quantities of temporal conditions stored in databases. Small errors in bookkeeping or in properly specifying which data to use in the code are difficult to detect. To validate the modeling of the lepton identification, acceptances, and triggering we use a calibration that is predicted to better than 1.5% and is directly sensitive to errors affecting overall efficiencies for leptons and $\not\!\!E_{\mathrm{T}}$. We measure the ratio R [see Eq. (1)] of inclusively produced W and Z bosons in their respective leptonic decay channels [29].

The ratio R has been calculated at NNLO by Berends *et al.*, and is predicted to be 10.67 ± 0.15 [27]. We measure $R = 10.52 \pm 0.04(\mathrm{stat})$ using electrons and $10.46 \pm 0.05(\mathrm{stat})$ using muons. The observed numbers agree with the theoretical prediction within 2%, a negligible difference relative to the other systematic uncertainties on the $t \to Zc$ measurement.

IX. THE FCNC ANALYSIS

Assuming that the FCNC decay of the top quark $t \to Zc$ is nonzero, a $t\bar{t}$ pair can decay to $WbWb$, $WbZc$, or $ZcZc$ with decay rates proportional to $(1 - \mathrm{Br}(t \to Zc))^2$, $2\,\mathrm{Br}(t \to Zc) \cdot (1 - \mathrm{Br}(t \to Zc))$, and $\mathrm{Br}(t \to Zc)^2$, respectively. W and Z bosons are well identified via only their leptonic decay modes, which have small branching fractions. To keep acceptances high we require one of the bosons from the $t\bar{t}$ pair to decay leptonically and the other hadronically.

To avoid large systematic uncertainties, we analyze simultaneously two final states from decays of top-quark pairs: $p\bar{p} \to t\bar{t} \to ZcWb \to \ell\ell cjjb$ and $p\bar{p} \to t\bar{t} \to WbWb \to \ell\nu bjjb$, where ℓ is a lepton (e or μ), j is a jet, ν is a neutrino inferred via missing transverse energy ($\not\!\!E_{\mathrm{T}}$), b and c are "heavy-flavor" jets formed by hadronization of a bottom quark or a charm quark, respectively. This is done by comparing the number of expected events from SM $t\bar{t}$ decays and SM backgrounds to the number of observed events in each final state. The contributions from $t\bar{t}$ decays depend on two numbers: $\mathrm{Br}(t \to Zc)$ and $N_{t\bar{t}} = \sigma(p\bar{p} \to t\bar{t}) \int Ldt$, where $\sigma(p\bar{p} \to t\bar{t})$ is the cross section of top-quark pair production at CDF and $\int Ldt$ is the integrated luminosity.

Additional discrimination against SM backgrounds is achieved by requiring at least one of the four jets in the final state to be consistent with originating from a heavy-flavor quark (b or c quark). The identification of a heavy-flavor jet is performed with the "b-tagging" algorithm which is introduced earlier in Sec. IV D.

The unknown structure of the FCNC coupling is parametrized via the polarization of the Z boson produced in $t \to Zc$ decay, as the polarization is the only parameter that affects the acceptance of FCNC top-quark decays. We vary the value of the longitudinal polarization of the Z bosons from 0.0 to 1.0. The final result is presented as a function of the longitudinal polarization.

We reconstruct the invariant mass of the top quark, M_{top}, in events with two leptons and four jets assuming that the events are $t\bar{t}$ FCNC decays. The distribution of M_{top} provides additional separation between standard model backgrounds and the FCNC signal; the top-quark mass, M_{top}, distribution for background events peaks below the FCNC signal.

X. MEASURING TOP-QUARK PAIR PRODUCTION IN EVENTS WITH A W BOSON AND FOUR JETS

The measurement of the FCNC branching ratio relies on two data sets (see Sec. III): $\ell\ell$ + 4 jets and $\ell\not\!\!E_{\mathrm{T}}$ + 4 jets, where $\ell\ell$ and $\ell\not\!\!E_{\mathrm{T}}$ are consistent with decays of a Z boson or a W boson (see Secs. V and VI), respectively. In this section we focus only on events with $\ell\not\!\!E_{\mathrm{T}}$ + 4 jets, where the majority comes from $t\bar{t} \to WbWb$ decays. At least one of the four jets in the final state is required to be identified as HF decay by the secondary vertex identification algorithm. The estimate of SM production of W + HF events (e.g., $W + b\bar{b}$) requires normalization of three key components: $t\bar{t}$; $W + b\bar{b}$, $W + c\bar{c}$, $W + c$; and "non-W" background events, which arise from mismeasured jet events.

A. Estimating the contributions from $t\bar{t}$ production, W + HF production, and from non-W backgrounds

The dominant SM contribution to the W + 4-jet bin with one jet identified as heavy flavor (a "b tag") is $t\bar{t}$ production. The production of a W boson with heavy flavor, $W + b\bar{b}$, $W + c\bar{c}$, and $W + c$, however, dominates production in the $W + 2$ jet bin. We consequently use the spectrum in the number of jets in W + HF production to estimate the contribution from $t\bar{t}$ alone in an iterative process. We take the top-quark pair production cross section to be $\sigma(t\bar{t}) = 7.6$ pb [50].

We initially assume that the fraction of non-W events is negligible. We determine the normalization of the standard model contribution to the W + HF processes $W + b\bar{b}$, $W + c$, and $W + c\bar{c}$ by rescaling the respective cross sections to match the total number of events observed in the $W + 2$ jets bin. We assume that the overall normalization of $W + b\bar{b}$ + jets, $W + c\bar{c}$ + jets, and $W + c$ + jets can be corrected by a single scale factor that is the same for the electron and muon channels.

We then use this normalization of the W + HF samples to estimate the remaining contribution from non-W's, as described in detail below in Sec. X B.

We then repeat the calculation of the fraction of real W + HF events using the estimate of non-W's, rescaling of the W + HF by a factor of 0.97 ± 0.09 to match the number of events in the $W + 2$ jets bin. The final jet multiplicity distributions for the W + HF sample are shown in Fig. 7. We find good agreement for events with three or more jets in the W + HF sample.

The motivation for normalizing to the 2-jet multiplicity bin is based on the matrix-element structure of associated heavy-flavor production in W and Z events. A problem with any normalization scheme that uses the 1-jet bin is that different diagrams contribute to the $N = 1$ and the $N = 2$ jet multiplicity bins; taking into account the (large, particularly for charm) NLO corrections is tricky since the corrections differ significantly for the different processes. In contrast, the radiation of additional jets and jet matching procedures in the higher-multiplicity jet bins are fairly well understood [53] in comparison to the uncertainties in the 1-jet bin. We avoid these issues by normalizing the multijet multiplicity distribution to the 2-jet bin.

We perform an additional consistency check by comparing a measured top-quark pair production cross section with its theoretical prediction, assuming that there are no FCNC [54]. In the W + 4-jet bin the ratio of the measured cross section to the SM expectation is 1.17 ± 0.09, where the SM background is evaluated using a top-quark cross section of 7.6 pb and $\mathrm{Br}(t \to Wb) = 100\%$ (i.e., $\mathrm{Br}(t \to Zc) = 0$). The H_T distribution for the W + 4 jets events agree well with those of top-quark pair decays (see Fig. 8), where the contribution from the top-quark pair production is normalized with the measured cross section. The total transverse energy, H_T, is a scalar sum of E_T of all reconstructed objects (electrons, muons, photons, jets, missing transverse energy, and unclustered energy). The transverse energies of the objects are the same as those used for the calculation of the missing energy $\not\!\!E_{\mathrm{T}}$ in the event.

B. Non-W backgrounds in the $t\bar{t}$ sample

The same procedure used for measuring background in the inclusive W bosons sample (see Sec. VII D) is used to measure backgrounds in the $t\bar{t}$ sample. The number of misidentified W bosons (non-W's) is estimated by fitting the $\not\!\!E_{\mathrm{T}}$ distribution for each jet multiplicity bin in events with one tight lepton and M_{trans} higher than 20 GeV, where the transverse mass M_{trans} is calculated for the lepton and

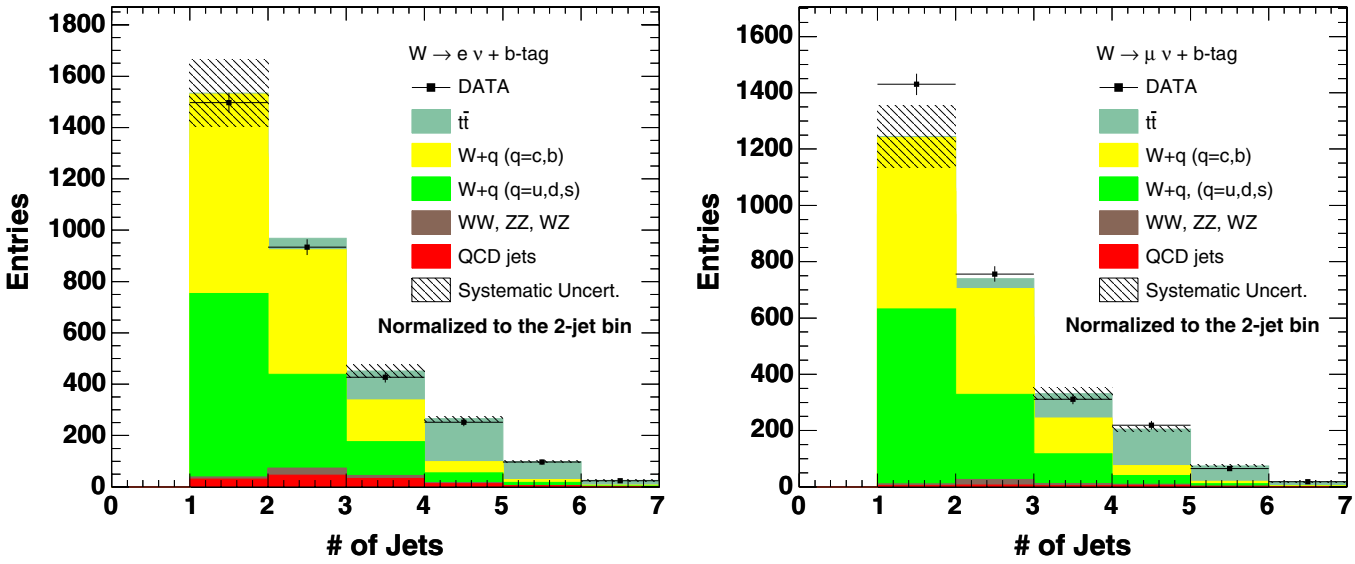

FIG. 7 (color online). The measured distributions (points) in the number of jets in events with a W and a b tag for $W \to e\nu$ and $W \to \mu\nu$, compared to SM expectations (histogram). The order of stacking in the histograms is the same as in their legends.

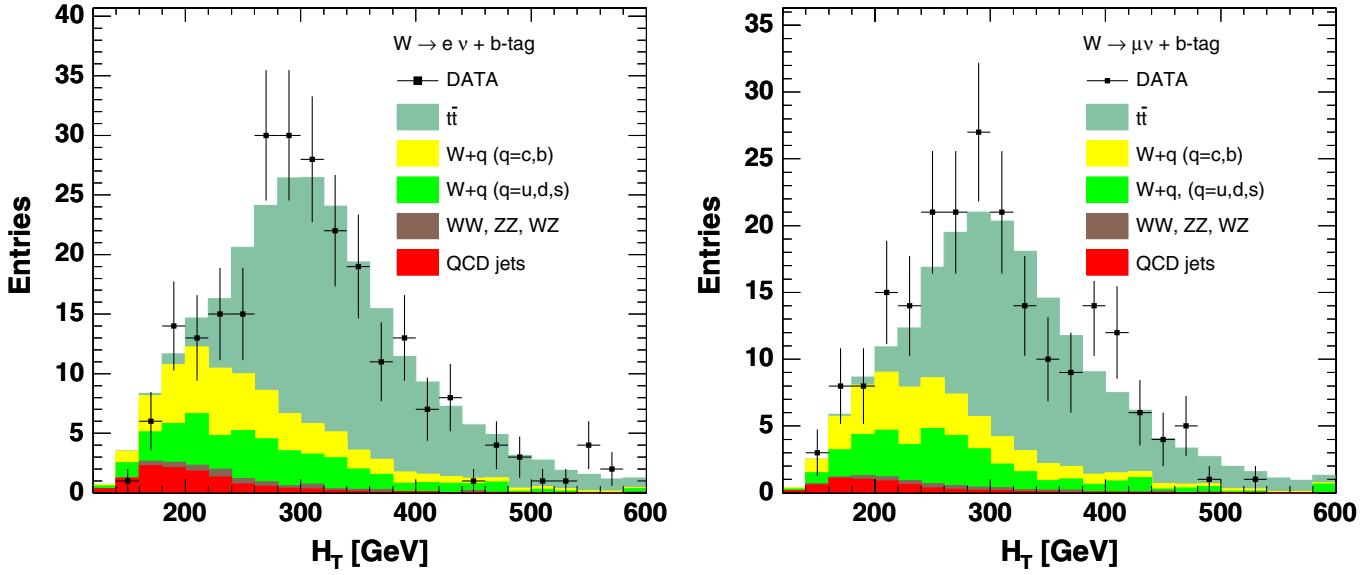

FIG. 8 (color online). The measured distribution (points) in H_T in events with a W and a b tag, compared to SM expectations (histogram), for the electron channel (left figure) and muon channel (right figure). The order of stacking in the histograms is the same as in their legends.

$\not\!\!E_{\mathrm{T}}$. The fractions of non-W events obtained after applying the $\not\!\!E_{\mathrm{T}}$ cut ($\not\!\!E_{\mathrm{T}} > 25$ GeV) are presented in Table II versus the jet multiplicity [55].

The acceptance times efficiency, $A_{WW\to\ell\not\!\!E_{\mathrm{T}}}$ (see Subsec. XI A), is determined from the MC simulations of the standard model $t\bar{t}$ decays for the $W + 4$ jets bin. The obtained numbers are presented in Table III. The cumulative acceptances $A_{WW\to\ell\not\!\!E_{\mathrm{T}}}$ include the branching fractions for $W \to \ell\nu$ and $W \to qq'$ decays.

TABLE II. The fractions of non-W QCD background (labeled as QCD jets in Fig. 7) in events with a tight lepton (e or μ), $\not\!\!E_{\mathrm{T}} > 25$ GeV, $M_{\mathrm{trans}}(\ell + \not\!\!E_{\mathrm{T}}) > 20$ GeV, and at least one b-tagged jet.

Jet Multiplicity	1 jet	2 jets	3 jets	≥ 4 jets
$W \to e\nu$ + jets	2.0%	4.9%	7.6%	4.7%
$W \to \mu\nu$ + jets	0.3%	0.9%	1.3%	2.6%

TABLE III. The acceptance times efficiency for $\ell\not\!\!E_{\mathrm{T}} + 4$ jets events which are produced via $t\bar{t} \to WbWb \to \ell\not\!\!E_{\mathrm{T}} + 4$ jets decay chain (see Subsec. XI A). The efficiencies are calculated from the Monte Carlo simulations and corrected to match the lepton identification and triggering efficiencies in data.

Process	$A_{WW\to\ell\not\!\!E_{\mathrm{T}}}$
$t\bar{t} \to WbWb \to e\not\!\!E_{\mathrm{T}} + 4$ jets	0.0128
$t\bar{t} \to WbWb \to \mu\not\!\!E_{\mathrm{T}} + 4$ jets	0.00994

TABLE IV. A summary of the numbers of $W + 4$ jets events. At least one jet in each event is required to be b tagged.

Final state	Observed	Background (non-$t\bar{t}$)
$e\not\!\!E_{\mathrm{T}} + 4$ jets	252	98.7
$\mu\not\!\!E_{\mathrm{T}} + 4$ jets	219	75.2

C. Summary of the backgrounds in $W + 4$ jets

The number of events observed and the expected number from all processes except $t\bar{t}$ production are given in Table IV.

XI. THE CONTRIBUTION FROM FCNC DECAYS OF $t\bar{t}$ PAIRS TO EVENTS WITH W/Z BOSONS AND JETS

A. Acceptances for $t\bar{t}$ decays

We use a modified version of the MADGRAPH Monte Carlo event generator [56] to produce simulated events for the $t\bar{t} \to ZcWb$ and $t\bar{t} \to ZcZc$ processes, which are then hadronized using PYTHIA.

In order to calculate the rates of expected events for the two final states $\ell\ell + 4$ jets and $\ell\not\!\!E_{\mathrm{T}} + 4$ jets, we need to introduce a notation for the acceptances multiplied by efficiencies, $(A \cdot \epsilon)_{\mathrm{Y}}$, for the decay chain "Y" of $t\bar{t}$ pairs. Acceptance $(A \cdot \epsilon)_{\mathrm{Y}}$ is a fraction of $t\bar{t}$ events observed in the corresponding final state. The acceptances $(A \cdot \epsilon)_{\mathrm{Y}}$ include combinatoric factors and the corresponding branching fractions for decays of W's and Z's: Br($W \to \ell\nu$), Br($W \to qq'$), Br($Z \to \ell\ell$), and Br($Z \to q\bar{q}$).

The acceptances $(A \cdot \epsilon)_{\mathrm{Y}}$ depend on the FCNC branching ratio Br($t \to Zc$). We divide the acceptances by polynomials dependent on Br($t \to Zc$) to factor out the terms independent of the FCNC branching ratio:

$$A_{ZZ\to\ell\ell} = \frac{(A\cdot\epsilon)_{t\bar{t}\to ZcZc\to\ell\ell+4\text{ jets}}}{\mathrm{Br}(t\to Zc)^2}, \quad (2)$$

$$A_{ZW\to\ell\ell} = \frac{(A\cdot\epsilon)_{t\bar{t}\to ZcWb\to\ell\ell+4\text{ jets}}}{\mathrm{Br}(t\to Zc)\cdot(1-\mathrm{Br}(t\to Zc))}, \quad (3)$$

$$A_{WZ\to\ell\not{E}_T} = \frac{(A\cdot\epsilon)_{t\bar{t}\to ZcWb\to\ell\nu+4\text{ jets}}}{\mathrm{Br}(t\to Zc)\cdot(1-\mathrm{Br}(t\to Zc))} + \frac{(A\cdot\epsilon)_{t\bar{t}\to ZcWb\to\ell\not{E}_T+4\text{ jets}}}{\mathrm{Br}(t\to Zc)\cdot(1-\mathrm{Br}(t\to Zc))}, \quad (4)$$

$$A_{WW\to\ell\not{E}_T} = \frac{(A\cdot\epsilon)_{t\bar{t}\to WbWb\to\ell\nu+4\text{ jets}}}{(1-\mathrm{Br}(t\to Zc))^2}, \quad (5)$$

and

$$A_{ZZ\to\ell\not{E}_T} = \frac{(A\cdot\epsilon)_{t\bar{t}\to ZcZc\to\ell\not{E}_T+4\text{ jets}}}{\mathrm{Br}(t\to Zc)^2}. \quad (6)$$

The values of A_Y are determined using simulated samples where all the $t\bar{t}$ pairs decay exclusively to only one of the intermediate states: $WbZc$, $ZcZc$, or $WbWb$. The acceptance $A_{WZ\to\ell\not{E}_T}$ includes two decay chains since the missing energy, $\not{E}_T$, can be produced via decay $W\to\ell\nu$ or by misidentifying $Z\to\ell\ell$ decay. The $Z\to\ell\ell$ decay can be mistaken for a $W\to\ell\nu$ decay when one of the two leptons is not identified (i.e., missing). The loss of the real lepton can create significant missing energy.

B. Properties of the FCNC $t\to Zc$ coupling

We note that the helicity structure of a possible $t\to Zc$ vertex is model dependent. We cover the full range of possible helicities so as to be assumption independent.

The kinematic properties of $t\to Zc$ decay are reflected by the angular distributions of the decay products. This affects the total acceptance for the FCNC events since the isolation requirement is placed on all the identified jets and leptons. For example, the final state of the $t\to Zc\to\ell\ell c$ decay chain can be fully described by introducing an angle θ^*, taken to be the angle between the direction of the top quark (anti-top quark) and the positive (negative) lepton in the rest frame of the Z boson. The angular distribution of θ^* has the following general form:

$$f(\theta^*) = a_0\cdot f_0(\theta^*) + a_1\cdot f_1(\theta^*) + a_2\cdot f_2(\theta^*), \quad (7)$$

where a_0, a_1, and a_2 are constants which depend on the polarization of the Z boson and whose sum is 1 ($a_0+a_1+a_2=1$). The functions $f_i(\theta^*)$ are given by

$$f_0(\theta^*) = \tfrac{3}{4}(1-\cos^2(\theta^*)), \quad (8)$$

$$f_1(\theta^*) = \tfrac{3}{8}(1+\cos(\theta^*))^2, \quad (9)$$

and

$$f_2(\theta^*) = \tfrac{3}{8}(1-\cos(\theta^*))^2. \quad (10)$$

The angular distribution of decay products of the $t\to Wb\to\ell\nu b$ decay is parametrized with the same function $f(\theta^*)$ by taking appropriate values of the a_i. In the case of $t\to Wb$ decay the coefficients a_0, a_1, and a_2 are the fractions of longitudinal, left-handed, and right-handed helicities of the W boson, respectively. However, the Z boson, unlike the W boson, has both right-handed and left-handed couplings. Consequently, while the coefficient a_0 is simply the fraction of the longitudinally-polarized Z bosons, the coefficients a_1 and a_2 are linear functions of the fractions of left-handed and right-handed helicities of the Z boson.

The distribution of $\cos(\theta^*)$ resulting from an arbitrary FCNC coupling can always be described by choosing appropriate values for the constants a_i. The acceptances of the FCNC top-quark decays A_Y depend on the angular distributions of the decay products since we require the isolation in a cone of 0.4 for all the identified leptons and jets. In consequence, the acceptances are functions of a_0 and a_1 (i.e., $A_Y = A_Y(a_0, a_1)$, noting that $a_2 = 1-a_0-a_1$). The top-quark decay is symmetric with respect to the charge of the fermion ($\ell\bar{\ell}$ or $q\bar{q}$), and therefore the acceptances calculated for decays of right-handed Z bosons and left-handed bosons are identical. This means that the acceptances A_Y can be fully parametrized with the fraction of longitudinally-polarized Z bosons (i.e., $A_Y = A_Y(a_0, 1-a_0) = A_Y(a_0)$).

We compute each acceptance A_Y for five values of the fraction of longitudinally-polarized Z bosons using Monte Carlo simulated events. This allows us to calculate the acceptances A_Y for any fraction a_0 by interpolating the acceptances A_Y between the points measured. The acceptance $A_{WW\to\ell\not{E}_T}$ is a constant since it does not have any FCNC vertices. The other acceptances, $A_{ZZ\to\ell\ell}$, $A_{ZW\to\ell\ell}$, $A_{WZ\to\ell\not{E}_T}$, and $A_{ZZ\to\ell\not{E}_T}$ have linear or quadratic dependences on the fraction of the longitudinal helicity of the Z bosons:

$$A_{ZZ\to\ell\ell}(a_0) = a_0^2\cdot A^{\mathrm{long}}_{ZZ\to\ell\ell} + 2\cdot a_0\cdot(1-a_0)\cdot A^{\mathrm{corr}}_{ZZ\to\ell\ell} + (1-a_0)^2\cdot A^{\mathrm{left}}_{ZZ\to\ell\ell}, \quad (11)$$

$$A_{ZW\to\ell\ell}(a_0) = a_0\cdot A^{\mathrm{long}}_{ZW\to\ell\ell} + (1-a_0)\cdot A^{\mathrm{left}}_{ZW\to\ell\ell}, \quad (12)$$

$$A_{WZ\to\ell\not{E}_T}(a_0) = a_0\cdot A^{\mathrm{long}}_{WZ\to\ell\not{E}_T} + (1-a_0)\cdot A^{\mathrm{left}}_{WZ\to\ell\not{E}_T}, \quad (13)$$

and

$$A_{ZZ\to\ell\not{E}_T}(a_0) = a_0^2\cdot A^{\mathrm{long}}_{ZZ\to\ell\not{E}_T} + 2\cdot a_0\cdot(1-a_0)\cdot A^{\mathrm{corr}}_{ZZ\to\ell\not{E}_T} + (1-a_0)^2\cdot A^{\mathrm{left}}_{ZZ\to\ell\not{E}_T}, \quad (14)$$

where A^{long}_Y are measured for the longitudinally-polarized component of the Z decays, A^{left}_Y are for the left-handed

component, and the value of $A_{\Upsilon}^{\mathrm{corr}}$ is obtained using FCNC events where the Z bosons are mixed with 50% left-handed and 50% longitudinal polarizations. The acceptance $A_{ZZ\to\ell\ell}$ has a quadratic dependence on a_0 since it accounts for the two FCNC decays of the top and antitop quarks. The numerical values of the acceptances are tabulated in Secs. X and XII.

XII. MEASURING THE CONTRIBUTIONS FROM FCNC AND SM PROCESSES IN EVENTS WITH A Z BOSON AND FOUR JETS

At this stage we consider only events which have two leptons consistent with a parent Z boson and at least one b-tagged jet. We use the jet multiplicity distribution (see Fig. 9) to constrain the number of non-SM $Z+4$-jet events. We do this by scaling the total $Z+$ HF component, $Z+q$ ($q=c,b$), to the number of (observed-mistagged) $Z+2$ jets events in the electron and muon modes simultaneously. The fraction of mistagged, $Z+q$ ($q=u,d,s$), events is estimated from data using inclusive $Z+$ jets events (see Sec. IV D).

The number of $Z+4$ jets events observed and the expected number from all SM processes are given in Table V.

The FCNC signal contribution is divided into two parts, $ZcWb$ and $ZcZc$, since the b-tagging rates are different. We summarize the acceptance and the efficiency measurements for the $Z+4$ jets channel in Tables VI, VII, VIII, and IX. The case when a leptonic decay of a Z boson is misidentified as the leptonic decay of a W boson is taken into account in Tables VIII and IX.

The top-quark mass M_{top} is used as a discriminating variable against the SM backgrounds as was mentioned earlier in Sec. IX. More details on the calculation of M_{top} are provided later in the section. We recalculate the acceptances $A^{i}_{ZZ\to\ell\ell}$ and $A^{i}_{ZW\to\ell\ell}$ for the ith bin of the top-quark mass distribution by multiplying a cumulative acceptance A_{Υ} (Υ is $ZZ\to\ell\ell$ or $ZW\to\ell\ell$) and the fraction of events in the ith bin:

TABLE V. A summary of the numbers of $Z+4$ jets events. At least one jet in each event is required to be b tagged.

Final state	Observed	SM background
e^+e^-+4 jets	6	8.4
$\mu^+\mu^-+4$ jets	8	6.9

TABLE VI. The acceptance times efficiency for the dilepton signature from the inclusive FCNC decay of $t\bar{t}\to ZcZc\to\ell\ell+ccjj$ for different values of the longitudinal fraction of Z bosons, for electron pairs and muon pairs separately. The SM branching ratios for the $Z\to\ell\ell$ decays are included.

Process	$A_{ZZ\to\ell\ell}$
The longitudinal fraction is $a_0=0.00$.	
$t\bar{t}\to ZcZc\to e^+e^-+4$ jets	0.00185
$t\bar{t}\to ZcZc\to\mu^+\mu^-+4$ jets	0.00178
The longitudinal fraction is $a_0=0.50$.	
$t\bar{t}\to ZcZc\to e^+e^-+4$ jets	0.00203
$t\bar{t}\to ZcZc\to\mu^+\mu^-+4$ jets	0.00192
The longitudinal fraction is $a_0=1.00$.	
$t\bar{t}\to ZcZc\to e^+e^-+4$ jets	0.00222
$t\bar{t}\to ZcZc\to\mu^+\mu^-+4$ jets	0.00205

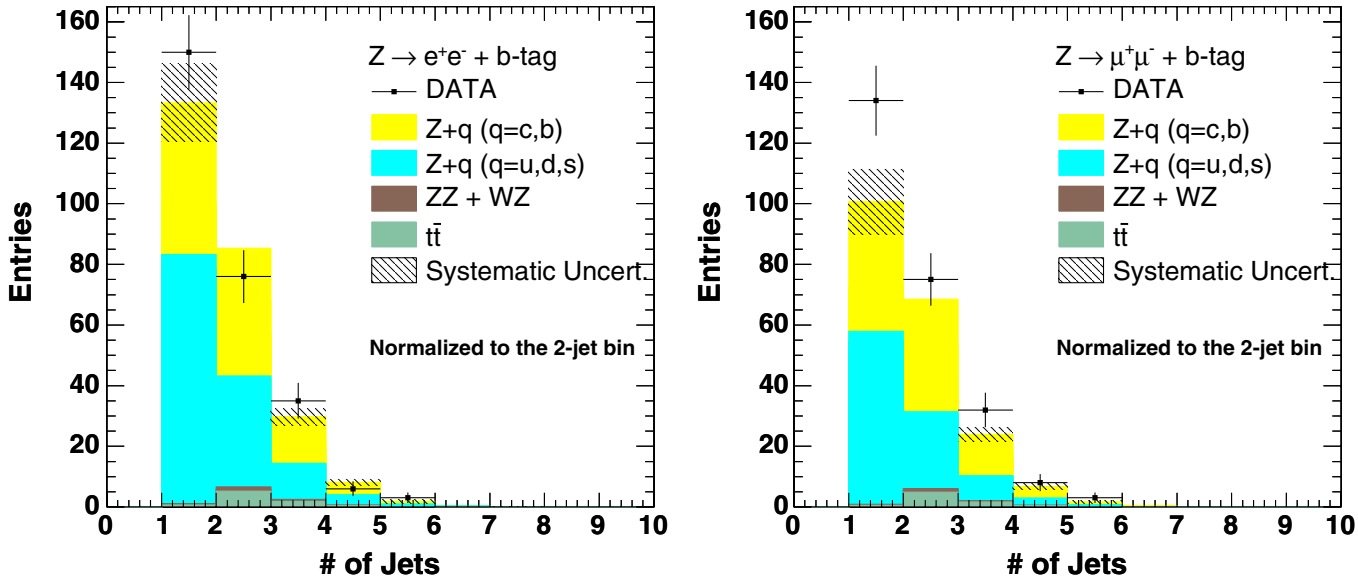

FIG. 9 (color online). The measured distribution (points) in the number of jets in events with a Z and a b tag, compared to SM expectations (histogram), for the electron channel (left figure) and muon channel (right figure). We normalize to the average of the $Z\to e^+e^-$ and $Z\to\mu^+\mu^-$ 2-jet bins. The order of stacking in the histograms is the same as in their legends.

TABLE VII. A summary of the acceptance times efficiency for the dilepton signature from inclusive FCNC decays of $t\bar{t} \to ZcWb \to \ell\ell + bcjj$, for different values of the longitudinal fraction of Z bosons, for electron pairs and muon pairs separately.

Process	$A_{ZW\to\ell\ell}$
The longitudinal fraction is $a_0 = 0.00$.	
$t\bar{t} \to ZcWb \to e^+e^- + 4$ jets	0.00275
$t\bar{t} \to ZcWb \to \mu^+\mu^- + 4$ jets	0.00267
The longitudinal fraction is $a_0 = 1.00$.	
$t\bar{t} \to ZcWb \to e^+e^- + 4$ jets	0.00313
$t\bar{t} \to ZcWb \to \mu^+\mu^- + 4$ jets	0.00293

$$A_{\mathrm{Y}}^{i} = A_{\mathrm{Y}} \cdot \frac{N_i}{\sum_k N_k}. \tag{15}$$

The obtained acceptances A_{Y}^{i} depend on the reconstructed top-quark mass of the $t\bar{t}$ FCNC events.

We reconstruct the value of M_{top} for each candidate event that contains at least two leptons consistent with a parent Z boson and at least four jets. The procedure is very similar to that of the CDF top-quark mass measurement [57].

The value of M_{top} is calculated by minimizing the χ^2 distribution, which is based on the assumption that the event is $p\bar{p} \to t\bar{t} \to Z + 4$ jets $\to \ell\ell + 4$ jets. The minimization takes into account every combination of the jets in the event since we do not know the true jet-parton assignments. To do so we loop through all possible permutations and select the one with the lowest χ^2. The top-quark mass distribution obtained for $t\bar{t} \to ZcZc \to \ell\ell + 4$ jets decays does not differ significantly from that of $WbZc$ decay. The exact formula for the χ^2 has the following structure:

TABLE VIII. A summary of the acceptance times efficiency for the contribution to the single lepton + $\not\!\!E_{\mathrm{T}}$ signature from the inclusive FCNC decays of $t\bar{t} \to WbZc \to \ell\not\!\!E_{\mathrm{T}} + bcjj$ (i.e., the decay of a Z boson is misidentified as the decay of a W boson) and $t\bar{t} \to WbZc \to \ell\nu + bcjj$. Standard model branching ratios are included. The acceptance $A_{WZ\to\ell\not\!\!E_{\mathrm{T}}}$ is the sum of acceptances for the decay modes which contribute to the signature of $\ell + \not\!\!E_{\mathrm{T}} + 4$ jets.

Process	$A_{WZ\to\ell\not\!\!E_{\mathrm{T}}}$
The longitudinal fraction is $a_0 = 0.00$.	
$t\bar{t} \to WbZc \to e\nu + 4$ jets	0.00927
$t\bar{t} \to WbZc \to e\not\!\!E_{\mathrm{T}} + 4$ jets	0.00179
$t\bar{t} \to WbZc \to \mu\nu + 4$ jets	0.007915
$t\bar{t} \to WbZc \to \mu\not\!\!E_{\mathrm{T}} + 4$ jets	0.002180
The longitudinal fraction is $a_0 = 1.00$.	
$t\bar{t} \to WbZc \to e\nu + 4$ jets	0.00967
$t\bar{t} \to WbZc \to e\not\!\!E_{\mathrm{T}} + 4$ jets	0.00185
$t\bar{t} \to WbZc \to \mu\nu + 4$ jets	0.00817
$t\bar{t} \to WbZc \to \mu\not\!\!E_{\mathrm{T}} + 4$ jets	0.00227

TABLE IX. The acceptance times efficiency for the contribution to the single lepton + $\not\!\!E_{\mathrm{T}}$ signature from the inclusive FCNC decay of $t\bar{t} \to ZcZc \to \ell + \not\!\!E_{\mathrm{T}} + ccjj$, where at least one dileptonic decay of Z boson has been misidentified as the decay of a W boson. Standard model branching ratios are included. Note that this channel depends on the square of the FCNC branching ratio for the Z, and so its contribution is suppressed relative to that from the case where only one Z decays by FCNC (see Table VIII).

Process	$A_{ZZ\to\ell\not\!\!E_{\mathrm{T}}}$
The longitudinal fraction is $a_0 = 0.00$.	
$t\bar{t} \to ZcZc \to e + \not\!\!E_{\mathrm{T}} + 4$ jets	0.000873
$t\bar{t} \to ZcZc \to \mu + \not\!\!E_{\mathrm{T}} + 4$ jets	0.00127
The longitudinal fraction is $a_0 = 0.50$.	
$t\bar{t} \to ZcZc \to e + \not\!\!E_{\mathrm{T}} + 4$ jets	0.000858
$t\bar{t} \to ZcZc \to \mu + \not\!\!E_{\mathrm{T}} + 4$ jets	0.00132
The longitudinal fraction is $a_0 = 1.00$.	
$t\bar{t} \to ZcZc \to e + \not\!\!E_{\mathrm{T}} + 4$ jets	0.000838
$t\bar{t} \to ZcZc \to \mu + \not\!\!E_{\mathrm{T}} + 4$ jets	0.00137

$$\begin{aligned}\chi^2(M_{\mathrm{top}}) = &\sum_{\ell_1,\ell_2,\mathrm{jets}} \frac{(\hat{E}t_i - Et_i)^2}{\sigma_i^2} + \sum_{x,y} \frac{(\hat{E}t_i^{\mathrm{uncl}} - Et_i^{\mathrm{uncl}})^2}{\sigma_i^2} \\ &+ \frac{(M(j_1j_2) - M_W)^2}{\Gamma_W^2} + \frac{(M(l^+l^-) - M_Z)^2}{\Gamma_Z^2} \\ &+ \frac{(M(W + j) - M_{\mathrm{top}})^2}{\Gamma_{\mathrm{top}}^2} + \frac{(M(Z + j) - M_{\mathrm{top}})^2}{\Gamma_{\mathrm{top}}^2}.\end{aligned} \tag{16}$$

The first term contains the fitted transverse energies of the leptons and four jets within the corresponding experimental resolutions. The second term includes the x and y components of the unclustered energy. The expression also contains terms for the reconstructed masses of the W, Z, and the two top quarks (i.e., $t \to Zc \to \ell\ell$ jet and $t \to Wb \to 3$ jets). The χ^2 function includes all the top-specific corrections of jet-energy scales and energy resolutions used in the single-lepton top-quark mass measurement [57].

We process the $Z + 4$ jets events from data and simulation samples with the same top-quark mass fit computer code so that we can compare the M_{top} distributions between data, the SM expectations, and a hypothetical FCNC signal. The comparison is shown in Fig. 10; the data agree well with the SM background distribution.

In the following section we describe the evaluation of the systematic uncertainties that go into making this statement quantitative and setting a limit on a FCNC signal.

XIII. SYSTEMATIC UNCERTAINTIES

We discuss separately the systematic uncertainties involving the acceptances and backgrounds in the following two subsections.

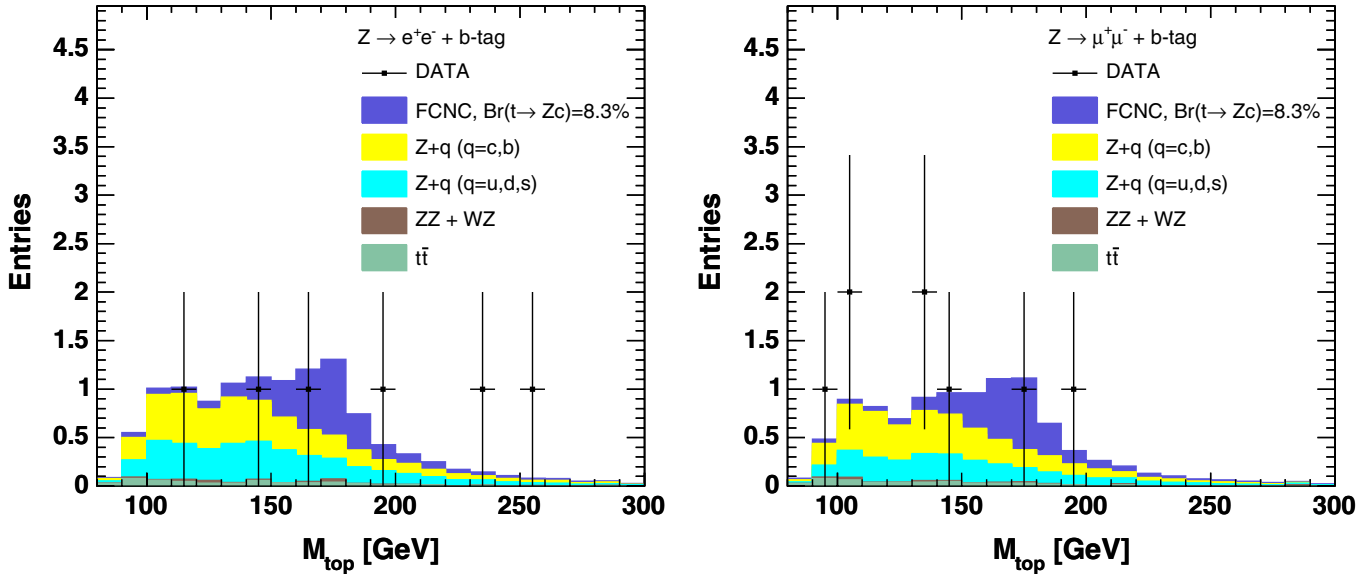

FIG. 10 (color online). The measured distribution (points) in the fitted top-quark mass in events with a Z and four jets with at least one b-tagged jet, compared to the SM expectations and an FCNC signal (stacked histogram), for the electron channel (left figure) and muon channel (right figure). The branching fraction for the FCNC signal is taken from Table XII. The order of stacking in the histograms is the same as in their legends.

A. Systematic uncertainties on the acceptances

The uncertainties on the five acceptances used in determining the limit, A_Y, defined in Sec. IX, are summarized in Table X. For each of the A_Y the effect of uncertainties in the jet-energy scale, initial and final state radiation, lepton identification efficiencies, parton distribution functions, and the identification ("tagging") of bottom quarks and charm quarks have been taken into account.

To estimate the systematic uncertainty from each of these sources, we vary each of the parameters listed below by 1 standard deviation ($\pm\sigma$) and recalculate the acceptances A_Y. The effect of the uncertainty for each of the sources is correlated among the A_Y, and these correlations are taken into account in the limit-setting procedure.

Of the two acceptances that contribute to the signatures containing two charged leptons, $A_{ZZ\to\ell\ell}$ and $A_{ZW\to\ell\ell}$, the latter dominates as it depends linearly on the FCNC branching ratio of the Z boson, while the contribution corresponding to $A_{ZZ\to\ell\ell}$ enters as the square. In a similar fashion, the single lepton + $\not\!\!E_T$ signature is dominated by the SM decay of the top-quark pair into $W^+W^-b\bar{b}$, with an acceptance $A_{WW\to\ell\not\!\!E_T}$, as there is no FCNC branching ratio in the rate. The process described by $A_{WZ\to\ell\not\!\!E_T}$ is suppressed by a single factor of the FCNC branching ratio, while that described by $A_{ZZ\to\ell\not\!\!E_T}$ is quadratic, and hence makes a very small contribution.

The largest systematic uncertainties in the dominant processes in the dilepton and single-lepton modes are the uncertainties in the efficiency for identifying b and c quarks. For b quarks, we follow the prescription used previously in CDF studies of the top quark, and use a systematic uncertainty on the tagging efficiency of 5%

TABLE X. A summary table of the systematic uncertainties on the acceptances. Correlations are taken into account in the calculation of the limit. The abbreviation "lept" stands for the systematic uncertainty due to lepton identification and triggering.

Systematic uncertainty in %	$\frac{\delta(A_{ZZ\to\ell\ell})}{A_{ZZ\to\ell\ell}}$	$\frac{\delta(A_{ZW\to\ell\ell})}{A_{ZW\to\ell\ell}}$	$\frac{\delta(A_{WZ\to\ell\not\!\!E_T})}{A_{WZ\to\ell\not\!\!E_T}}$	$\frac{\delta(A_{WW\to\ell\not\!\!E_T})}{A_{WW\to\ell\not\!\!E_T}}$	$\frac{\delta(A_{ZZ\to\ell\not\!\!E_T})}{A_{ZZ\to\ell\not\!\!E_T}}$
Jet energy scale	2.5	2.6	2.7	2.4	6.4
ISR	0.5	0.5	0.5	0.5	0.5
FSR	0.6	0.6	0.6	0.6	0.6
PDF's	0.9	0.9	0.9	0.9	0.9
HF quark ID	10.2	5.0	5.0	4.1	10.6
ID and triggering of electrons	1.6	1.6	0.1	0.1	0.1
or					
ID and triggering of muons	2.8	2.8	0.9	0.9	0.9
Total	10.6 ⊕ lept	5.8 ⊕ lept	5.8 ⊕ lept	4.9 ⊕ lept	12.4 ⊕ lept

[42]. Similarly, for c quarks, we assign a 15% uncertainty [41].

The next largest contribution to the systematic uncertainties is from uncertainties in the calibration of jet energies [57]. The systematic uncertainties are positively correlated for all the A_Y.

The contributions from lepton identification and trigger efficiencies are limited by the precision check of the R ratio (see Sec. VIII). We assume that the reconstruction and the triggering efficiencies of electrons and muons are not correlated. We note that acceptances and trigger efficiencies are correlated for $W \to \ell\nu$ and $Z \to \ell\ell$ decays to leptons of the same flavor. This means that $A_{ZZ\to\ell\ell}$ would be misestimated by the same percentage as $A_{ZW\to\ell\ell}$ for leptons of the same flavor. The same holds true for $A_{WZ\to\ell\not{E}_T}$, $A_{WW\to\ell\not{E}_T}$, and $A_{ZZ\to\ell\not{E}_T}$.

The systematic uncertainties in the A_Y due to lepton identification and triggering are estimated using deviations between the measured cross sections of inclusive W's and Z's, used in calculating the ratio R, from their theoretical values:

$$\frac{\Delta\sigma(Z\to\ell\ell)}{\sigma(Z\to\ell\ell)} = -\frac{\delta(A_{ZZ\to\ell\ell})}{A_{ZZ\to\ell\ell}} = -\frac{\delta(A_{ZW\to\ell\ell})}{A_{ZW\to\ell\ell}} \quad (17)$$

and

$$\frac{\Delta\sigma(W\to\ell\nu)}{\sigma(W\to\ell\nu)} = -\frac{\delta(A_{WZ\to\ell\not{E}_T})}{A_{WZ\to\ell\not{E}_T}} = -\frac{\delta(A_{WW\to\ell\not{E}_T})}{A_{WW\to\ell\not{E}_T}} = -\frac{\delta(A_{ZZ\to\ell\not{E}_T})}{A_{ZZ\to\ell\not{E}_T}}. \quad (18)$$

The uncertainty on the integrated luminosity does not contribute at the first order to the measurement of $\mathrm{Br}(t\to Zc)$ since it is positively correlated between $\sigma(W\to\ell\nu)$ and $\sigma(Z\to\ell\ell)$.

The deviation of the measured R ratio is

$$\frac{\Delta R}{R} = \Delta\left(\frac{\sigma(W\to\ell\nu)}{\sigma(Z\to\ell\ell)}\right)\Big/\left(\frac{\sigma(W\to\ell\nu)}{\sigma(Z\to\ell\ell)}\right) = \frac{\Delta\sigma(W\to\ell\nu)}{\sigma(W\to\ell\nu)} - \frac{\Delta\sigma(Z\to\ell\ell)}{\sigma(Z\to\ell\ell)}. \quad (19)$$

Therefore, the connection between the deviation in the R ratio and the uncertainties of the A_Y is the following:

$$\frac{\Delta R}{R} = \delta\left(\frac{A_{ZW\to\ell\ell}}{A_{WW\to\ell\not{E}_T}}\right)\Big/\left(\frac{A_{ZW\to\ell\ell}}{A_{WW\to\ell\not{E}_T}}\right) = \frac{\delta(A_{ZW\to\ell\ell})}{A_{ZW\to\ell\ell}} - \frac{\delta(A_{WW\to\ell\not{E}_T})}{A_{WW\to\ell\not{E}_T}}. \quad (20)$$

We treat $\frac{\delta(A_{WW\to\ell\not{E}_T})}{A_{WW\to\ell\not{E}_T}}$ and $\frac{\delta(A_{ZW\to\ell\ell})}{A_{ZW\to\ell\ell}}$ as negatively correlated as it is the most conservative case. Also this treatment insures the constraint from the R ratio.

Contributions from other sources are significantly smaller than those from heavy-flavor identification and jet-energy scale. The effect of initial and final state radiation (ISR and FSR) on $A_{WW\to\ell\not{E}_T}$ was studied in Ref. [58]. We expect that FSR will contribute to the uncertainties in the other three A_Y in the same way since we require four jets in the final state for all four channels and the samples are triggered on leptons. The ISR uncertainty should also contribute identically to the uncertainties of the four acceptances A_Y. The uncertainties are found to be 0.5% for ISR and 0.6% for FSR, assumed to be 100% correlated across all A_Y.

The uncertainties arising from parton distribution functions (PDF's) can also propagate into the acceptances. However, the dominant effect of changes in the PDF's is on the production of the $t\bar{t}$ pairs and not on the decay kinematics. The effect of the uncertainties was also studied in Ref. [58]. The total uncertainty is 0.9% and is 100% correlated for the four A_Y.

B. Systematic uncertainties of the backgrounds

The sensitivity of this search for a Z boson and a charm quark coming from top-quark decay depends strongly on the understanding of SM W boson and Z boson production in conjunction with heavy flavor (W/Z + HF). We summarize the systematic uncertainties of backgrounds in both the single-lepton and dilepton signatures [the terms $B_{\ell\nu}$ and $B_{\ell\ell}$ in Eqs. (22) and (23)] in Table XI, and discuss them below.

The largest uncertainty in the background comes from modeling the production of W bosons and Z bosons accompanied by heavy-flavor and additional jets. The Z + HF and W + HF backgrounds are modeled by ALPGEN [59], and hadronized with PYTHIA [60]. The predictions suffer from uncertainties in the modeling procedure. In particular, the expected number of events in the W/Z + 4 jets category enters directly into the calculation for the final result. To make an estimate of the uncertainty on the expected number of W/Z + HF events, we assume that there is a set or parameters which allows ALPGEN to model the data precisely. A deviation from the "ideal set" can be estimated using inclusive Z + jets events with jet multiplicity below 3. A comparison between data and ALPGEN

TABLE XI. The relative systematic uncertainties (%) on the backgrounds for 4-jet semileptonic and dilepton final states of $t\bar{t}$ pairs. The contributions from uncertainties in the Monte Carlo modeling and in the rate of misidentified heavy-flavor jets (mistags) are (conservatively) taken to be correlated in the computation of the limit.

Systematic uncertainty in %	$\ell\not{E}_T$ + 4 jets	$\ell\ell$ + 4 jets
W/Z + HF + Jets MC modeling	20	20
Mistags	15	15
W/Z + HF Normalization	2.5	8

simulations is shown in Fig. 11. The observed deviation on the rate of radiation of one extra jet in the inclusive sample is less than 5%. We assume independent gluon emission, and so take 10% as the estimate of the uncertainty on this ALPGEN prediction for the radiation of 2 extra jets in the inclusive sample. However, the slopes of the N-jet distribution are predicted to be different in the inclusive and HF samples, with the factors for each additional jet being 5.0 and 2.7 in the inclusive and b-tagged samples, respectively. The ratio of 5.0 to 2.7 makes a relative difference of 1.85 between radiating an extra jet in inclusive and tagged samples. We consequently increase the 10% deviation by a factor of 2 (rounding 1.85 up), to 20%.

The sensitivity of the limit to the number of 4-jet Z + HF events was calculated by performing a set of "pseudo-experiments" with different levels of the systematic uncertainties of the backgrounds. The limit was calculated with this systematic uncertainty set to zero, set to 20% (nominal), and set to 40%. The respective shifts in the limit are -0.1%, zero (by construction), and $+0.1\%$, respectively. The weak dependence is caused by the measurement technique; we measure a ratio of top-quark events between $Z + 4$ jets and $W + 4$ jets final states. An increase in the number of background events leads to a decrease in the $t\bar{t}$ cross section measured with $W + 4$ jets events. Simultaneously it leads to a decrease in the upper limit on the number of FCNC signal events in the $Z + 4$ jets final state.

The method of predicting misidentified heavy flavor (mistags) by applying a parametrization of the rate for a light-quark jet or gluon jet being misidentified as a jet from a charm or bottom quark to jets in a sample before heavy-flavor identification contributes a significant systematic uncertainty to the background estimates. We vary the mistag probability calculated by the standard CDF algorithm used in the measurement of the top-quark cross section [58] jet-by-jet by $\pm 15\%$ (i.e., a factor of 0.85 or 1.15) to estimate the contribution to the uncertainty.

A smaller contribution to the uncertainty is due to the overall normalization of the predicted SM boson + HF contribution. The normalizations of the background distributions from W + HF and Z + HF events are treated as independent, and are chosen to match the number of observed events in the W + HF + 2 jets and Z + HF + 2 jets channels, respectively, as discussed in detail in Secs. X and XII. The finite statistics of the 2-jet bin of the data contributes an uncertainty of 2.5% to the single-lepton and dilepton signatures, respectively.

The 6% uncertainty of the measured luminosity affects only processes that are normalized absolutely: WW, WZ, and ZZ production. Consequently, the contribution from the uncertainty of luminosity to the final result is negligible ($< 0.1\%$).

XIV. STATISTICAL EVALUATION OF THE LIMITS ON Br($t \to Zc$)

At this point we have all the ingredients needed to evaluate limits on the FCNC branching ratio Br($t \to Zc$). The branching ratio is evaluated by comparing the numbers of expected and observed events in two final states, $\ell\ell$ + 4 jets and $\ell \not{E}_{\mathrm{T}}$ + 4 jets, using Poisson statistics. The num-

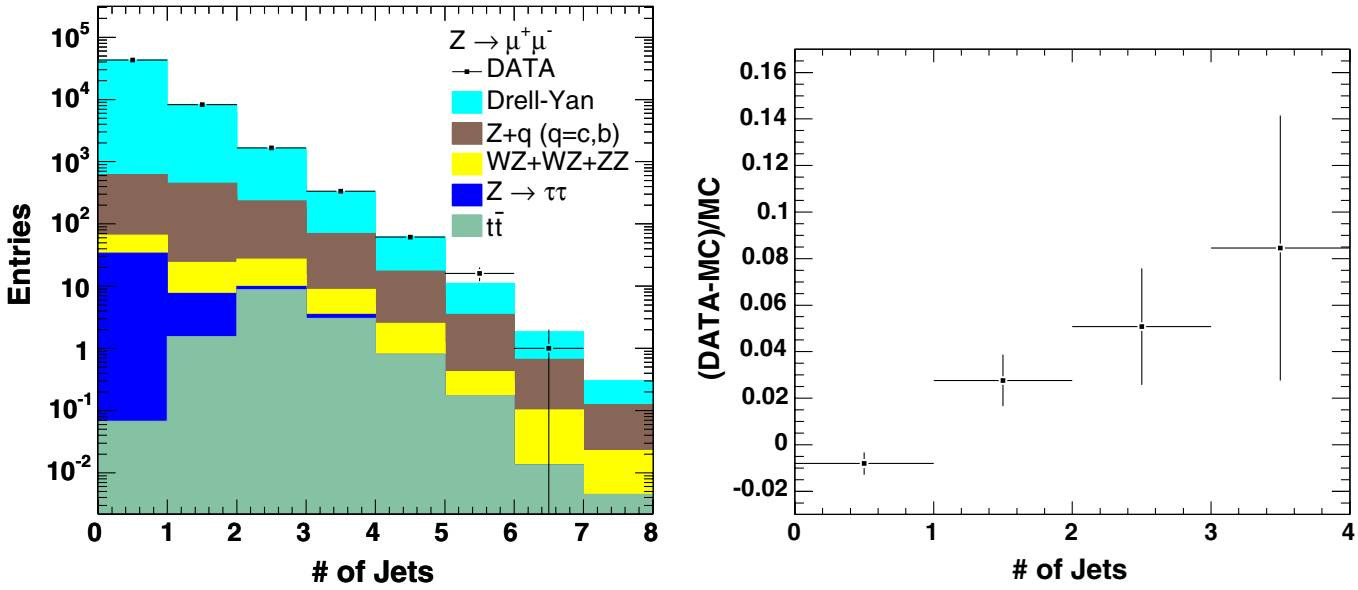

FIG. 11 (color online). The measured distribution (points) in the number of jets in events with an inclusive decay of $Z \to \mu^+\mu^-$, compared to SM expectations (stacked histogram). The order of stacking in the histogram is the same as in the legend. The Z + jets processes (Drell-Yan, $Z + b$, and $Z + c$) are modeled with ALPGEN. The right-hand plot shows the difference between the data and predictions.

bers of observed events are denoted as $N_{\ell\nu}$ and $N_{\ell\ell}$ for final states $\ell\not{E}_{\mathrm{T}} + 4$ jets and $\ell\ell + 4$ jets, respectively, the numbers of expected events are denoted as $X_{\ell\nu}$ and $X_{\ell\ell}$.

To avoid large systematic uncertainties, we simultaneously analyze two final states from decays of top-quark pairs: $p\bar{p} \to t\bar{t} \to ZcWb \to \ell\ell cjjb$ and $p\bar{p} \to t\bar{t} \to WbWb \to \ell\not{E}_{\mathrm{T}} bjjb$. This is done by comparing the number of expected events from SM $t\bar{t}$ decays and SM backgrounds to the number of observed events in each final state. The contributions from $t\bar{t}$ decays depend on two numbers: $\mathrm{Br}(t \to Zc)$ and $N_{t\bar{t}} = \sigma(p\bar{p} \to t\bar{t}) \int Ldt$, where $\sigma(p\bar{p} \to t\bar{t})$ is the cross section of top-quark pair production and $\int Ldt$ is the integrated luminosity. We treat $\mathrm{Br}(t \to Zc)$ and $N_{t\bar{t}}$ as free parameters in the calculation of the limit on the FCNC branching ratio. The result of the comparison is presented as a likelihood which is a 2-dimensional function of $\mathrm{Br}(t \to Zc)$ and $N_{t\bar{t}}$. We use the likelihood distribution to estimate limits on the FCNC branching ratio $\mathrm{Br}(t \to Zc)$ using a Bayesian approach.

For simplicity, let us consider the case in which we observe only two categories of events: $N_{\ell\nu}$ and $N_{\ell\ell}$, by applying some set of selection requirements. Later we will show how to generalize this approach to be used with more categories of selected events. This is done since we will consider events with electrons and muons separately and we use a binned distribution of M_{top} for $\ell\ell + 4$ jets events.

We assume that the top quark has only the two decay channels Wb and Zc, and so $\mathrm{Br}(t \to Wb) + \mathrm{Br}(t \to Zc) = 1$. The number of expected $t\bar{t}$ pairs is

$$N_{t\bar{t}} = \sigma(p\bar{p} \to t\bar{t}) \cdot \int Ldt, \tag{21}$$

where $\sigma(p\bar{p} \to t\bar{t})$ can be taken *a priori* since it is independent of any FCNC physics.

The expected numbers of events in each of the decay modes are estimated as follows, where we use the notation $B_Z = \mathrm{Br}(t \to Zc)$:

$$X_{\ell\nu} \approx B_{\ell\nu} + N_{t\bar{t}} A_{WW \to \ell\not{E}_{\mathrm{T}}} \tag{22}$$

and

$$X_{\ell\ell} \approx B_{\ell\ell} + N_{t\bar{t}} A_{ZW \to \ell\ell} \cdot B_Z. \tag{23}$$

The complete formulas are presented in [61]. In the formulas above $B_{\ell\nu}$ and $B_{\ell\ell}$ are non-top SM contributions (backgrounds) to final states $\ell\not{E}_{\mathrm{T}} + 4$ jets and $\ell\ell + 4$ jets, respectively; A_{Y} is acceptance for a decay mode Y (see Sec. IX).

The limit on the ratio $\mathrm{Br}(t \to Zc)$ is estimated using probability density (i.e., likelihood) function defined as

$$L(B_Z, N_{t\bar{t}}) = P(N_{\ell\nu}, N_{\ell\ell} | B_Z, N_{t\bar{t}}), \tag{24}$$

i.e.,

$$L(B_Z, N_{t\bar{t}}) = P(N_{\ell\nu} | X_{\ell\nu}) P(N_{\ell\ell} | X_{\ell\ell}), \tag{25}$$

where

$$P(N|X) = \frac{X^N e^{-X}}{N!} \tag{26}$$

is a Poisson distribution. The likelihood $L(B_Z, N_{t\bar{t}})$ is defined in the physical region of parameters $N_{t\bar{t}} \geq 0$ and $0 \leq B_Z \leq 1$.

The complete set of systematic uncertainties is included in the likelihood function using a Monte Carlo simulation which takes into account the correlations between the uncertainties.

To discriminate the FCNC signal from the expected SM background, we use the distribution in the reconstructed top-quark mass, M_{top}, for $Z + 4$ jets events. Events from the signal process should form a distinguishable peak at the top-quark mass. We combine probabilities for each bin of the reconstructed top-quark mass distribution

$$\prod_i P(N^i_{\ell\ell} | X^i_{\ell\ell}), \tag{27}$$

where the index i refers to the ith bin of the distribution in the top mass. This requires calculating the acceptances $A^i_{ZZ \to \ell\ell}$ and $A^i_{ZW \to \ell\ell}$ for each bin of the reconstructed top-quark mass histogram.

We note that the electron and muon decay modes of the top quarks are treated separately up to this point of the analysis in order to better understand the systematics of both. The two channels are then included together in the final likelihood function $L(B_Z, N_{t\bar{t}})$.

The likelihood function is used to construct a posterior probability density $P(B_Z|\mathrm{DATA})$, where DATA refers to the numbers of observed events, $N_{\ell\nu}$ and $N^i_{\ell\ell}$, in the electron and muon channels ($\ell = e$ or $\ell = \mu$). The posterior probability density function is converted into a limit on the FCNC branching ratio $\mathrm{Br}(t \to Zc)$ using a Bayesian approach.

A. Numerical computation of the likelihood distribution function $L(B_Z, N_{t\bar{t}})$

The observed distribution of the likelihood (computed for $t \to Zc$ decays where the Z bosons are 100% longitudinally polarized) is presented in Fig. 12.

A likelihood distribution is calculated for each given value of helicity of the $t \to Zc$ coupling since the acceptances A_{Y} vary for different structures of the FCNC coupling.

B. Computation of the posterior $P(\mathrm{Br}(t \to Zc)|\mathrm{DATA})$

The posterior probability density functions $P(B_Z|\mathrm{DATA})$ are computed from the likelihood functions $L(B_Z, N_{t\bar{t}})$ using a Bayesian approach as follows:

$$P(\mathrm{DATA}|B_Z) = \int_0^\infty L(B_Z, N_{t\bar{t}}) \cdot \pi_0(N_{t\bar{t}}) dN_{t\bar{t}} \tag{28}$$

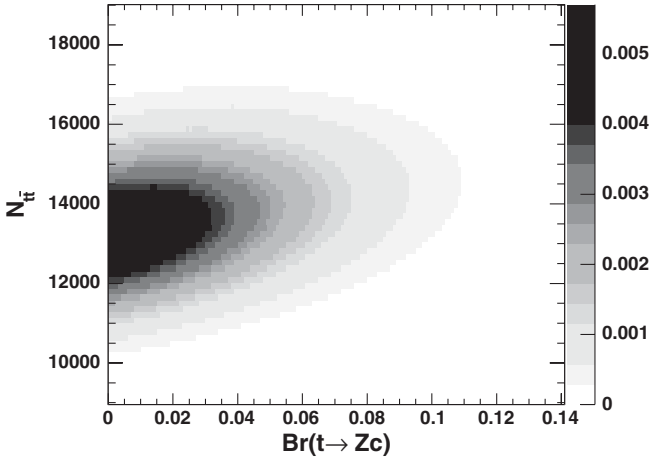

FIG. 12. The likelihood distribution $L(B_Z, N_{t\bar{t}})$ calculated as a function of $N_{t\bar{t}}$ and $B_Z = \mathrm{Br}(t \to Zc)$. The distribution is for FCNC decays of $t \to Zc$ with 100% longitudinally-polarized Z bosons.

$$P(B_Z|\mathrm{DATA}) = \frac{P(\mathrm{DATA}|B_Z) \cdot \pi_1(B_Z)}{\int_0^1 P(\mathrm{DATA}|B_Z) \cdot \pi_1(B_Z) dB_Z}, \quad (29)$$

where $\pi_0(N_{t\bar{t}})$ is the *a priori* probability density function of $N_{t\bar{t}}$ and $\pi_1(B_Z)$ is the *a priori* distribution of B_Z which is taken to be flat in the physical region (it is 1.0 for $0 \leq B_Z \leq 1$ and zero everywhere else). The distribution of $\pi_0(N_{t\bar{t}})$ represents the prior knowledge of the top pair production cross section, $\sigma(p\bar{p} \to t\bar{t})$.

We consider two choices of the $\pi_0(N_{t\bar{t}})$ prior distribution: flat and Gaussian. The flat distribution does not contain any information regarding the theoretical predictions of $\sigma(p\bar{p} \to t\bar{t})$. It is just a constant. The Gaussian distribution is derived using the theoretical estimates of the top pair production cross section $\sigma(p\bar{p} \to t\bar{t})$ [51] and the integrated luminosity. The theoretical estimate of the top pair production cross section is presented as a function of top-quark mass M_{top}. The measured top-quark mass is 170.9 ± 1.8 GeV [52]. The luminosity is 1.52 fb^{-1}, with an uncertainty of 6%. The Gaussian prior allows us to take into account the theoretical FCNC-independent knowledge of $\sigma(p\bar{p} \to t\bar{t})$.

The distribution for $P(B_Z|\mathrm{DATA})$, calculated for 100% longitudinally-polarized Z bosons, is shown in Fig. 13.

C. Computation of the upper limits on Br($t \to Zc$)

We use the posterior function $P(B_Z|\mathrm{DATA})$ to calculate the upper limit B_Z^{lim} on $\mathrm{Br}(t \to Zc)$ (i.e., B_Z) by solving the equation

$$\beta = \int_0^{B_Z^{\mathrm{lim}}} P(B_Z|\mathrm{DATA}) dB_Z, \quad (30)$$

where β is 0.95 (95% C.L). The upper limits versus the helicity of the Z boson are summarized in Table XII.

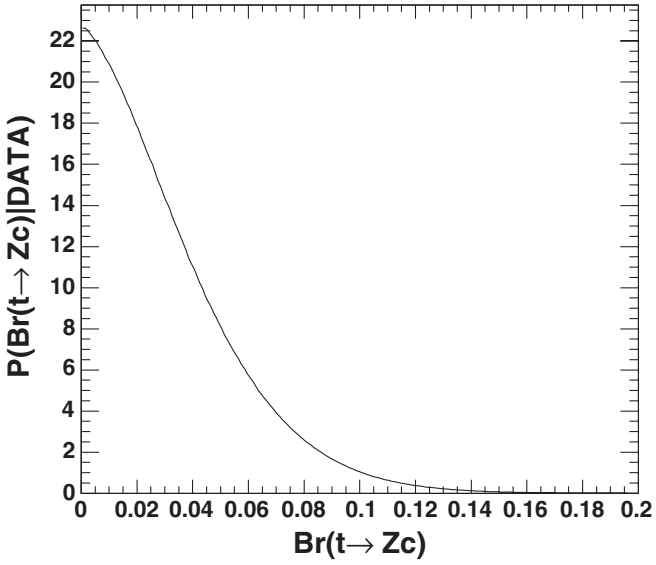

FIG. 13. The distribution for $P(\mathrm{Br}(t \to Zc)|\mathrm{DATA})$, calculated for 100% longitudinally-polarized Z bosons using the Gaussian prior.

TABLE XII. The upper limits on the FCNC branching ratio $\mathrm{Br}(t \to Zc)$ in % as a function of the longitudinal fraction of the Z bosons in the FCNC coupling ($t \to Zc$) at 95% C.L. The limits labeled Gaussian prior use as input the theoretical cross section of $\sigma(p\bar{p} \to t\bar{t})$; the limits labeled flat prior are theory independent.

Longitudinal fraction	0.00	0.25	0.50	0.75	1.0
Gaussian prior	9.0%	8.8%	8.6%	8.5%	8.3%
Flat prior	10.2%	10.0%	9.7%	9.5%	9.2%

We perform statistical cross-checks of the measured upper limits using pseudo-experiments. The pseudo-experiments are generated randomly assuming that there is no contribution from FCNC processes, i.e., by setting $\mathrm{Br}(t \to Zc) = 0$. The expected upper limit for 100% longitudinally-polarized Z's on $\mathrm{Br}(t \to Zc)$ is $8.7 \pm 2.6\%$, consistent with the observed limit of 8.3%.

XV. CONCLUSIONS AND RESULTS

Taking into account systematic uncertainties on Monte Carlo simulations, b tagging, mistag modeling, and lepton identification, we find an upper limit at 95% C.L. on the branching ratio of $t \to Zc$ of 8.3% for FCNC decays where the Z bosons are 100% longitudinally polarized. The result is primarily statistics limited. It can be significantly improved with more data if the number of $Z + 4$ jets events is high enough to do a shape analysis of the top-quark mass distribution.

To be assumption independent we parametrize the limit on $\mathrm{Br}(t \to Zc)$ as a function of the fraction of longitudinally-polarized Z bosons. The parametrization

allows us to cover the full range of all possible helicity structures of the $t \to Zc$ vertex. The upper limits are calculated at 95% C.L. for five fractions of longitudinally-polarized Z's using 1.52 fb^{-1} of data. The results are presented in Table XII for both the Gaussian and the flat priors. The limits vary between 8.3% and 9.0% for the Gaussian prior depending on the polarization of the Z boson and are about 1% less restrictive for the flat prior.

ACKNOWLEDGMENTS

We thank the Fermilab staff and the technical staffs of the participating institutions for their vital contributions. We thank Mary Heintz for unfailing computer support. We are grateful to Michel Herquet for explaining to us how to incorporate the FCNC couplings into MADGRAPH code, and then installing the model in MADGRAPH. This work was supported by the U.S. Department of Energy and National Science Foundation; the Italian Istituto Nazionale di Fisica Nucleare; the Ministry of Education, Culture, Sports, Science and Technology of Japan; the Natural Sciences and Engineering Research Council of Canada; the National Science Council of the Republic of China; the Swiss National Science Foundation; the A. P. Sloan Foundation; the Bundesministerium für Bildung und Forschung, Germany; the Korean Science and Engineering Foundation and the Korean Research Foundation; the Science and Technology Facilities Council and the Royal Society, UK; the Institut National de Physique Nucleaire et Physique des Particules/CNRS; the Russian Foundation for Basic Research; the Ministerio de Ciencia e Innovación, and Programa Consolider-Ingenio 2010, Spain; the Slovak R & D Agency; and the Academy of Finland.

[1] H. Fritzsch, Phys. Lett. B **224**, 423 (1989).
[2] C. Amsler *et al.*, Phys. Lett. B **667**, 1 (2008).
[3] J. Aguilar-Saavedra, Acta Phys. Pol. B **35**, 2695 (2004).
[4] F. Larios, R. Martinez, and M. A. Perez, Phys. Rev. D **72**, 057504 (2005).
[5] P. Fox *et al.*, Phys. Rev. D **78**, 054008 (2008).
[6] The CDF-II detector is described in more detail in many recent publications; see, for example, A. Abulencia *et al.* (CDF Collaboration), Phys. Rev. D **73**, 112006 (2006), and references therein.
[7] N. Cabbibo, in *Third Topical Conference on Proton-Antiproton Collider Physics, Rome 1983* (CERN 83-04, Geneva, 1983), p. 567; F. Halzen and M. Marsula, Phys. Rev. Lett. **51**, 857 (1983); K. Hikasa, Phys. Rev. D **29**, 1939 (1984); N. G. Deshpande *et al.*, Phys. Rev. Lett. **54**, 1757 (1985); A. D. Martin, R. G. Roberts, and W. J. Stirling, Phys. Lett. B **189**, 220 (1987); E. L. Berger, F. Halzen, C. S. Kim, and S. Willenbrock, Phys. Rev. D **40**, 83 (1989).
[8] E. Abouzaid and H. Frisch, Phys. Rev. D **68**, 033014 (2003).
[9] B. Cooper, Ph.D. thesis, University College London [Report No. FERMILAB-THESIS-2006-61, 2006].
[10] A. Messina (CDF Collaboration), Braz. J. Phys. **37**, 840 (2007).
[11] Transverse momentum and energy are defined as $p_T = p \sin\theta$ and $E_T = E \sin\theta$, respectively. Missing E_T ($\not\!\!E_T$) is defined by $\not\!\!E_T = -\sum_i E_T^i \hat{n}_i$, where i is the calorimeter tower number for $|\eta| < 3.6$ (see Ref. [12]), and $\hat{n}_i$ is a unit vector perpendicular to the beam axis and pointing at the ith tower. We correct $\vec{\not\!\!E}_T$ for jets, photons, electrons, and muons. We define the magnitude $\not\!\!E_T = |\vec{\not\!\!E}_T|$. We use the convention that momentum refers to pc and mass to mc^2.
[12] The CDF coordinate system is cylindrical and right handed, with the x axis horizontal and out of the Tevatron ring, the y axis up, the z axis along the proton beam, and $r = \sqrt{x^2 + y^2}$; ϕ is the azimuthal angle. The pseudorapidity $\eta \equiv -\ln(\tan(\theta/2))$, where θ is the polar angle; the η regions for detector components are defined with respect to the center of the detector. The central region is defined as $|\eta| < 1$.
[13] F. Abe *et al.* (CDF Collaboration), Phys. Rev. Lett. **80**, 2525 (1998).
[14] LEP Electroweak Working Group (EWWG), http://lepewwg.web.cern.ch/LEPEWWG/.
[15] T. Aaltonen *et al.* (CDF Collaboration), Phys. Rev. Lett. **101**, 192002 (2008).
[16] A. Sill *et al.*, Nucl. Instrum. Methods Phys. Res., Sect. A **447**, 1 (2000); A. Affolder *et al.*, Nucl. Instrum. Methods Phys. Res., Sect. A **453**, 84 (2000); C. S. Hill, Nucl. Instrum. Methods Phys. Res., Sect. A **530**, 1 (2004).
[17] A. Affolder *et al.*, Nucl. Instrum. Methods Phys. Res., Sect. A **526**, 249 (2004).
[18] T. Aaltonen *et al.* (CDF Collaboration), Phys. Rev. D **77**, 112001 (2008).
[19] L. Balka *et al.*, Nucl. Instrum. Methods Phys. Res., Sect. A **267**, 272 (1988).
[20] S. Kuhlmann *et al.*, Nucl. Instrum. Methods Phys. Res., Sect. A **518**, 39 (2004).
[21] D. Acosta *et al.* (CDF Collaboration), Phys. Rev. D **71**, 032001 (2005).
[22] M. G. Albrow *et al.* (CDF Collaboration), Nucl. Instrum. Methods Phys. Res., Sect. A **480**, 524 (2002).
[23] F. Abe *et al.*, Phys. Rev. Lett. **68**, 1104 (1992).
[24] G. Ascoli *et al.* (CDF Collaboration), Nucl. Instrum. Methods Phys. Res., Sect. A **268**, 33 (1988).
[25] T. Dorigo *et al.* (CDF Collaboration), Nucl. Instrum. Methods Phys. Res., Sect. A **461**, 560 (2001).
[26] D. Acosta *et al.* (CDF Collaboration), Nucl. Instrum. Methods Phys. Res., Sect. A **494**, 57 (2002).
[27] F. A. Berends *et al.*, Phys. Lett. B **224**, 237 (1989).
[28] P. Renton, arXiv:0804.4779.
[29] A. Abulencia *et al.* (CDF Collaboration), J. Phys. G **34**,

2457 (2007).
[30] For central electrons at least 5 hits in each of the 3 axial and 2 stereo layers of the COT are required.
[31] The fraction of electromagnetic energy allowed to leak into the hadron compartment E_{had}/E_{em} must be less than $0.055 + 0.00045 \times E_{em}(GeV)$ for central electrons, less than 0.05 for electrons in the end-plug calorimeters, less than $\max[0.125, 0.055 + 0.00045 \times E_{em}(GeV)]$ for photons.
[32] D. Acosta *et al.* (CDF Collaboration), Phys. Rev. D **71**, 051104 (2005).
[33] For tight muons at least 5 hits in each of the 3 axial and 3 stereo layers of the COT are required; for loose muons with a matching muon stub this is relaxed to 3 axial and 2 stereo layers. Loose muons without a matching stub have an additional cut on the χ^2 for the fit to the track.
[34] The energy deposited in the calorimeter tower traversed by the muon must be less than $2 + \max(0, 0.0115 \times (p - 100))$ GeV in the electromagnetic compartment and less than $6 + \max(0, 0.028 \times (p - 100))$ GeV in the hadronic compartment.
[35] A. V. Varganov, Ph.D. thesis, University of Michigan [Report No. FERMILAB-THESIS-2004-39, 2004].
[36] The muon stub in the muon systems must be within 7, 5, and 6 cm of the extrapolated COT track position, in the CMU, CMP, and CMX muon systems, respectively.
[37] A. V. Kotwal, H. K. Gerberich, and C. Hays, Nucl. Instrum. Methods Phys. Res., Sect. A **506**, 110 (2003).
[38] The maximum correction to the identification efficiency for central electrons is 1.7%, for plug electrons 6.3%, and for central muons 7.4%.
[39] F. Abe *et al.* (CDF Collaboration), Phys. Rev. D **45**, 1448 (1992).
[40] A. Bhatti *et al.*, Nucl. Instrum. Methods Phys. Res., Sect. A **566**, 375 (2006).
[41] A. A. Affolder *et al.* (CDF Collaboration), Phys. Rev. D **64**, 032002 (2001).
[42] D. Acosta *et al.* (CDF Collaboration), Phys. Rev. D **71**, 052003 (2005).
[43] The transverse mass is defined as $M_{trans}(\ell\nu) = \sqrt{2p_T(\ell)p_T(\nu)(1 - \cos(\phi(\ell) - \phi(\nu)))}$, where $p_T(X)$ is the transverse momentum of X (X is ℓ or ν) and $\phi(X)$ is the azimuthal angle of X.
[44] R. Field (CDF Collaboration), AIP Conf. Proc. **828**, 163 (2006); we use Tune A.
[45] We use Version 2.10 of ALPGEN.
[46] PYTHIA V6.216 with a $M(\gamma^*/Z) > 30$ GeV cut, Tune A, and the "Willis Sakumoto" corrections applied [47]. The Z + HF samples are produced with ALPGEN V2.10-PRIME (which has built-in MLM matching [48]) and showered with PYTHIA V 6.326. The both generators used CTEQ5L parametrization of the parton distribution functions.
[47] D. Acosta *et al.* (CDF Collaboration), Phys. Rev. Lett. **94**, 091803 (2005).
[48] M. L. Mangano, M. Moretti, F. Piccinini, and M. Treccani, J. High Energy Phys. 01 (2007) 013.
[49] J. M. Campbell and R. K. Ellis, Phys. Rev. D **60**, 113006 (1999).
[50] The theoretical estimate of the top pair production cross section is based on [51] using a top-quark mass of 170.9 ± 1.8 GeV [52].
[51] M. Cacciari *et al.*, J. High Energy Phys. 04 (2004) 068.
[52] CDF Collaboration and D0 Collaboration, Report No. Fermilab-TM-2380-E 2007; Report No. TEVEWWG/top 2007/01 2007.
[53] J. Alwall *et al.*, Eur. Phys. J. C **53**, 473 (2008).
[54] The scale factor for W + HF processes ($W + b\bar{b}$, $W + c\bar{c}$, and $W + c$) does not depend strongly on the number of $t\bar{t}$ events since the $t\bar{t} \to WbZc$ and $t\bar{t} \to WbWb$ modes contribute mostly to a final state with a W and three or four jets in the final state.
[55] The fit for $W \to \mu\nu$ + 4 jets with at least one jet b tagged returns zero events with a large uncertainty, due to the small statistics of the 4-jet sample. We consequently use the value of 2.6% obtained from the fit for inclusive $W \to \mu\nu$ + 4 jets, consistent with the fit.
[56] J. Alwall *et al.*, J. High Energy Phys. 09 (2007) 028.
[57] A. Abulencia *et al.* (CDF Collaboration), Phys. Rev. D **73**, 032003 (2006).
[58] A. Abulencia *et al.* (CDF Collaboration), Phys. Rev. D **74**, 072006 (2006).
[59] M. L. Mangano *et al.*, J. High Energy Phys. 07 (2003) 001.
[60] T. Sjostrand, L. Lonnblad, and S. Mrenna, arXiv:hep-ph/0108264.
[61] The complete formulas for the expected numbers of events are:

$$X_{\ell\nu} = B_{\ell\nu} + N_{t\bar{t}} \cdot \{(1 - B_Z)^2 \cdot A_{WW\to\ell\not{E}_T} + B_Z(1 - B_Z) \cdot (A_{WZ\to\ell\not{E}_T}) + B_Z^2 \cdot A_{ZZ\to\ell\not{E}_T}\} \quad (31)$$

and

$$X_{\ell\ell} = B_{\ell\ell} + N_{t\bar{t}} \cdot \{A_{ZW\to\ell\ell} \cdot B_Z + (A_{ZZ\to\ell\ell} - A_{ZW\to\ell\ell}) \cdot B_Z^2\}. \quad (32)$$